UiT
THE ARCTIC UNIVERSITY OF NORWAY

Department of Physics and Technology

Investigation of inflammatory response of macrophages and trophoblasts using structured illumination microscopy

—

Rajwinder Singh

FYS-3900 Master's Thesis in Physics

May 2017

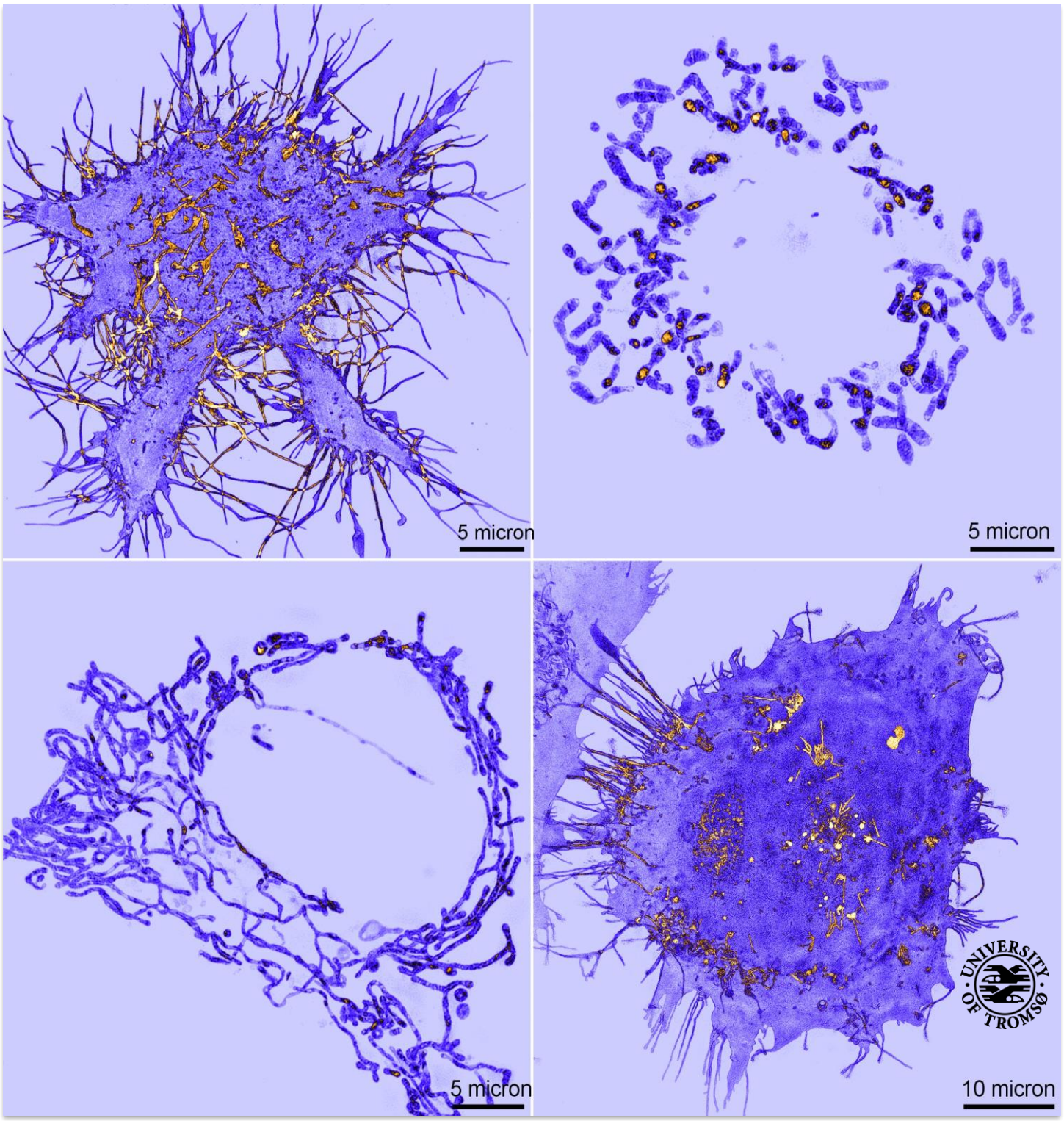

Acknowledgements

I came to study in Norway through the Quota Scholarship Scheme. Living in Norway and doing my master study at UiT-The Arctic University of Norway was a great experience. The atmosphere at the Optical Nanoscopy research group at Department of Physics and Technology, UiT, has always been very motivating and friendly. The group has been a great place for both social activities and scientific discussions. The research I have done during my master thesis has been a joint effort and I would like to thank few people here.

Assoc. Prof. Balpreet S. Ahluwalia, my supervisor. You gave me an opportunity to work on this project that let me discover the possibilities of structured illumination microscopy. Your constant supervision as well as essential information provided regarding my work was a great support in completing this project.

Prof. Purusotam Basnet, my co-supervisor. Being from a physics background, working in biology was difficult, but your calm and helping nature made it exciting and fun. Thanks to you I could build a unique relationship with biology, that I hope will last longer.

Dr. Deanna Wolfson, my co-supervisor. I took the first steps towards biology under your supervision. Thank you for training me in cell culture and OMX-SIM operation. Our meetings were always very encouraging and your optimism often helped me to continue to improve experimental methods. I also learnt a lot about presentation skills from you. I am highly indebted to you for your supervision during my master thesis.

Prof. Ganesh Acharya, Department of Clinical Science, Intervention and Technology, Karolinska Institutet, Sweden. Your critical comments and suggestions about my work have been very useful.

Azeem Ahmed and Vishesh Dubey, visiting PhD candidates at UiT from Indian Institute of Technology, Delhi for building quantitative phase microscope setup. This setup was used by Vishesh Dubey to acquire and analyse quantitative phase images of the samples provided by me, which are included in this thesis.

Dr. Cristina, Øystein and Ida from the Optical Nanoscopy research group at Department of Physics and Technology, UiT, for their useful suggestions during my experiments.

I want to extend sincere thanks to my mother and brother for their moral support. Their warmth of love is always felt by me.

Finally, I owe a lot to my late father for providing a me good education which formed a strong foundation for my higher studies. I learnt a lot in my early life from him and I am sure that he would be happy to see what I am doing at present.

Abstract

Approximately 800 women die from pregnancy or childbirth-related pregnancy complications around the world every day. One of the major reasons for these complications is inflammation following infection. Approximately 40% cases of preterm births occur due to microbial invasion in the genitourinary track. During inflammation, macrophages present at the feto-maternal junction release an increased amount of nitric oxide (NO) and other important pro-inflammatory cytokines: TNF-α and INF-γ. This can disturb the trophoblast function which can lead to pregnancy complications, such as abortion, pre-eclampsia and birth defects.

Here I aimed to study the cellular and sub-cellular morphological changes in macrophages (RAW264.7) and trophoblasts (HTR-8/SVneo) following externally supplied inflammatory agents: lipopolysaccharides (LPS), concanavalin-A (Con-A) and tumor necrosis factor alpha (TNF-α), in vitro.

Nitric oxide (NO) produced by the cells under inflammatory response was measured quantitatively using the Griess reagent test. Morphological changes were examined in response to LPS, Con-A and TNF-α challenge on live macrophages and trophoblasts using structured illumination microscopy (SIM) and quantitative phase microscopy (QPM).

LPS-challenged macrophages produced approximately 22 folds more NO as compared to controls, whereas no significant increase was seen after TNF-α or Con-A-challenge. No significantly increased amount of NO was detected in trophoblasts following LPS, TNF-α or Con-A-challenge. Superoxide ($O_2^{\cdot -}$) produced during respiration by mitochondria may react with NO to produce reactive nitrogen species (RNS) e.g. peroxynitrite ($ONOO-$), which have strong damaging effects on the mitochondria.

SIM imaging showed changes in the morphology of mitochondria and plasma membrane in approximately $50-60\%$ of macrophages following LPS challenge ($1\mu g/ml$ for $24hr$), but no detectable changes in mitochondria or plasma membrane were observed after TNF-α ($1ng/ml$ for $24hr$) or Con-A challenge ($1\mu g/ml$ for $24hr$). QPM revealed that the phase value decreased by approximately 18% in LPS-challenged macrophages after $24hr$ as compared to controls. In contrast, mitochondrial morphology appeared different in trophoblasts following TNF-α challenge under similar conditions. No effect was seen in trophoblast morphology following either LPS or Con-A challenge. Through SIM and QPM it was found that the effect on the morphology of macrophages can be detected following $2hr$ of incubation with LPS, whereas The Griess method was unable to detect increased amounts of NO before $4hr$.

Our results suggest that the cells which are responsible for the mother-fetus crosstalk, especially macrophages and trophoblasts, respond differently to various inflammatory agents. Additionally, SIM and QPM are shown to be live-cell friendly, useful tools to evaluate sub-cellular mechanisms associated with inflammation mediated pregnancy complications.

Contents

List of Figures

List of abbreviations

- SIM: Structured Illumination Microscopy
- QPM: Quantitative Phase Microscopy
- LPS: Lipopolysaccharides
- Con-A: Concanavalin-A
- TNF-α: Tumor Necrosis Factor-alpha
- INF-γ: Interferon gamma
- NO: Nitric Oxide
- iNOS: inducible Nitric Oxide Synthase
- CMG: CellMask Green
- MTG: MitoTracker Green
- ROS: Reactive Oxygen Species
- RNS: Reactive Nitrogen Species

Chapter 1

Introduction

"There is a unique pain that comes from preparing a place in your heart for a child that never comes." ∼ David Platt

Maternal infections can lead to pregnancy complications and failure like birth defects, intrauterine growth restriction, premature delivery, abortion etc.[1] According to the World Health Organisation (WHO), 830 women died everyday worldwide in 2015 due to pregnancy complications and childbirth related problems.[2] One of the major pathogen causing these infections is gram negative bacteria. These bacteria colonise the genitourinary tract of women, where they continuously release an endotoxin called lipopolysaccharide (LPS). LPS is present on the outer membrane of the gram negative bacteria which induces inflammation by stimulating the immune system, particularly macrophages.[3] In response to these stimuli, pro-inflammatory cytokines like TNF-α, INF-γ and the inflammatory modulators such as nitric oxide, etc. are released which are known to cause inflammation and infection. This can change the placental physiology during pregnancy, which can lead to preterm delivery in the rodents and is also linked to cause pregnancy related complications in humans.[4] It has also been shown in the research that increase in the number of the inflammation inducing macrophages at the feto-maternal junction can cause improper trophoblast invasion, which might lead to preeclampsia.[5]

The mechanisms linking infection to the placental dysfunction are still insufficiently understood.[6] Despite the advancements in Obstetrics and Neonatology, the rate of premature delivery has increased approximately 12% since 1990.[7] It is well-established fact that the macrophages and the trophoblast cells carry the receptors on their membrane that recognises the endotoxin.[8] However, very little is known about the effect of the endotoxin and other cytokines released in its effect on the morphology of these cells at the sub-cellular level. Many important details in the inflammation-related sub-cellular processes in these cells could so far not properly be observed due to the limited spatial resolution of conventional fluorescence microscopes. These limitations can be overcome using optical nanoscopes, such as SIM which improves the resolution twice as compared to the conventional microscopes and is compatible with the live cell imaging. Therefore, exploring the inflammatory response of the trophoblasts and the macrophages using optical nanoscopy can reveal unprecedented new insights into the understanding of pregnancy related complications and thus the potential of early detection and treatment.

Work done during my master thesis stands at the crossroads between physics and biology. *Fig1.1* provides an overview of the experiments done during my master thesis research. Macrophage and trophoblast cell lines were studied in parallel. Both the cell lines were challenged with three inflammatory agents (LPS, TNF-α and Concanavalin-A (Con-A)) as shown in *Fig1.1*. Different measurement techniques were employed to study the inflammatory response.

Having no prior practical knowledge of working in the field of biology, I was first trained in cell culture, sample preparation for the imaging and SIM operation during the first semester. During second semester, I independently did the following: cultured two cell lines, namely, HTR-

8/SVneo and RAW264.7; nitric oxide (NO) measurements in cell culture media using Greiss reagent; planned the experiments which were to be done using SIM and QPM; prepared the samples for SIM and QPM imaging; optimised the staining parameters; operated OMX-SIM to acquire images and analysed the images. QPM images were acquired and analysed by Vishesh Dubey, a visiting PhD candidate at UiT. Extensive studies were carried in studying macrophages following $24hr$ challenge with LPS. Due to the lack of time, studies in inflammatory response of macrophages at early time-point are not complete and further experiments need to be done. Due to the same reason, inflammatory response of trophoblasts was studied following $24hr$ challenge with inflammatory agents only using SIM. Early time-point studies and quantitative analysis could not be done.

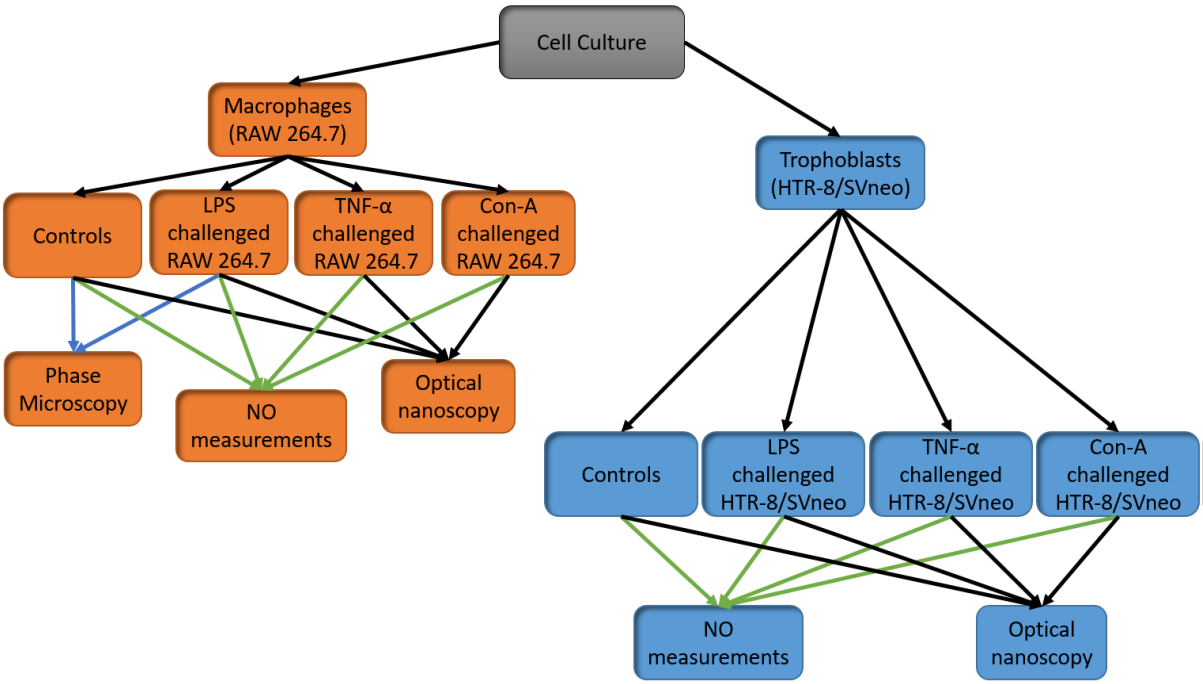

Figure 1.1: Experimental plan: Flow chart giving an overview of the various experiments performed to study the inflammatory response of macrophages and trophoblasts.

Currently I am working on the preparation of two manuscripts for peer-reviewed journals. I will be first author in one of them, and third author in the other. I have also submitted abstract for an oral presentation at International Federation of Placental Associations 2017 conference to be held in Manchester and I am co-author in another abstract submitted for an invited talk at the same conference.

Chapter 2

Theory and background

"Life is like a placenta. Full of attachment, separation and loss." ∼ Anonymous

Optical microscopy is a minimally invasive technique to study the cellular structure and processes. Initially, the high power microscopes were developed by Carl Zeiss and Ernst Abbe together in late 1800s, which had optical resolution around $0.2\mu m$ [9]. These microscopes formed the bases of the modern cell biology and microbiology. However, these microscopes have not been a choice when it comes to observing structures at the sub-cellular level. Light microscopy has a unique advantage, e.g. live cell imaging, over the other techniques like electron microscopy, when it comes to biological imaging. It's been only about two decades that the resolution limit has been broken and Nobel prize was given to Eric Betzig, Stefan W. Helland William E. Moerner for the development of super-resolved fluorescence microscopy. Now a days it is possible to build microscopes which have a resolution as low as 30 nm. These microscopes are called super-resolution microscopes or optical nanoscopes.

2.1 Point spread function and optical resolution

Any object to be imaged undera microscope e.g. biological cell might some times have a complex structure, containing substructures of varying sizes. Some of the organelles e.g. nucleus can be observed under an ordinary microscope, but others e.g. mitochondria, tubulin, etc. can't be observed through ordinary microscope.

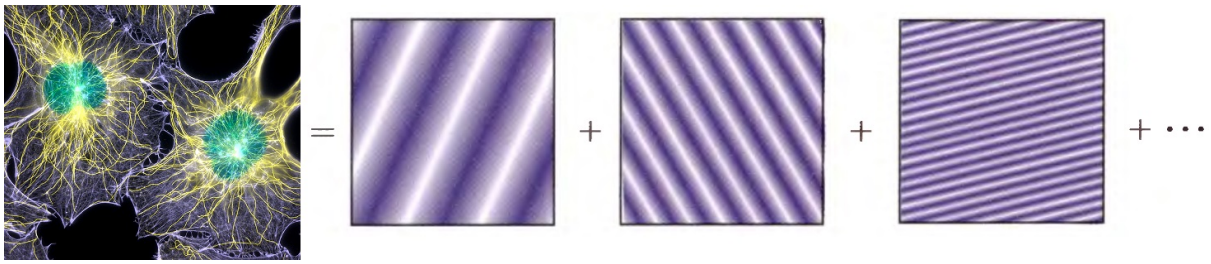

Figure 2.1: Any object to be imaged can be considered as the sum of different spatial frequencies and complex amplitudes. [10]

According to Fourier theory, any function (in our case an object to be imaged) can be analysed as the sum of harmonic functions of different spatial frequencies and complex amplitudes (*Fig2.1*). Spatial frequency can be defined as how many times a structure is varied in an interval of unit length. Higher the spatial frequency, the finer structural details become.

Consider an optical imaging system in which, an object lying at the focal plane of an objective lens and the tube lens lying behind the objective lens forms an image. The objective lens produce Fourier transform of the object at its back focal plane. Light corresponding to

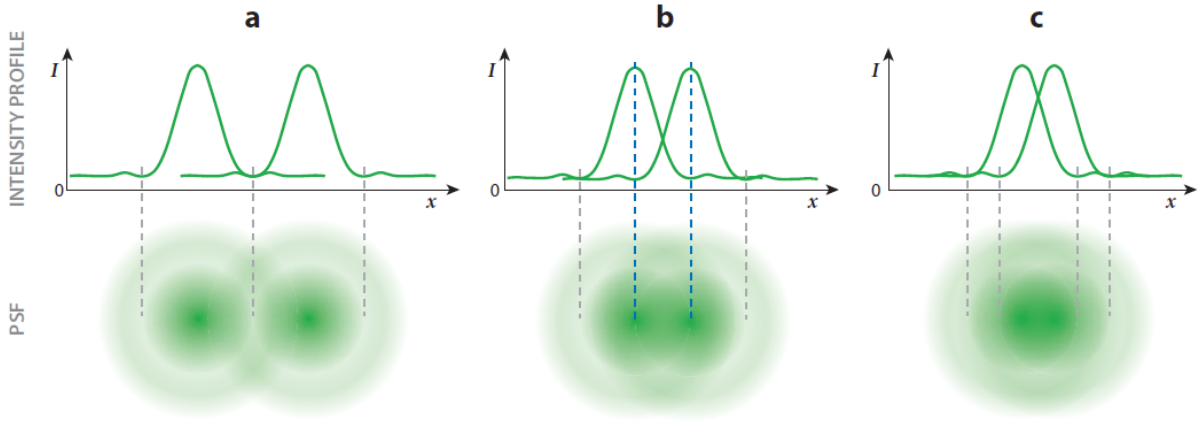

Figure 2.2: Rayleigh's criteria for resolution limit. (a) Well resolved point objects. (b) Just resolved point objects. (c) Unresloved point objects. [11]

the higher spatial frequencies are diffracted at larger angles, so these will not be collected by the lens. Hence, lens acts as a low pass filter. Tube lens converges these frequencies and the image of the object might be blurred due to missing fine details. If the object is a point object, its image will be a three dimensional blob and is called point spread function (PSF). PSF in two dimensions is known as airy pattern. *Fig2.2* represent PSF of two point objects lying at different distances. The Fourier transform of the PSF is known as optical transform function (OTF). The OTF of an optical system specifies which spacial frequencies are permitted through an optical system.

2.1.1 Rayleigh's criteria

Optical resolution is the ability of an optical system to resolve fine details of an object being imaged. If two point objects are placed at some distance r apart at the focal plane of an objective lens, the image will be two point spread functions. Upon decreasing the distance r between the objects, the PSFs will start overlapping and a point will be reached where the central maxima of one disk lies on the first minima of the other and vice-versa. At this distance r_l, the objects are just resolved and this distance is known as Rayleigh's resolution limit. Object lying further apart are well resolved and those lying closer than r_l will be unresolved (*Fig2.2*). According to Rayleigh, the resolution limit is given by:

$$r_l = \frac{1.22\lambda}{2N.A.} \tag{2.1}$$

where λ is the wavelength of light illuminating the sample, $N.A. = n\ sin\alpha$ is numerical aperture of the objective lens, n is the refractive index between sample and α is its edge angle. Resolution limit also gives us maximum cut-off spacial frequency,

$$\mathbf{k}_{max} = \frac{4\pi N.A.}{1.22\lambda} \tag{2.2}$$

that can be allowed to pass through the system. Eq(2.1) represent the lateral resolution which is typically, $r_l = 200nm$ for the conventional optical microscopes.

2.1.2 Surpassing the resolution limit-superresolution

For many years, resolution limit remained unbreakable. Researchers tried different methods to increase the resolution of microscopes. Going to lower wavelengths, such as particle waves was one of the options because higher the momentum, the shorter is the wavelength associated

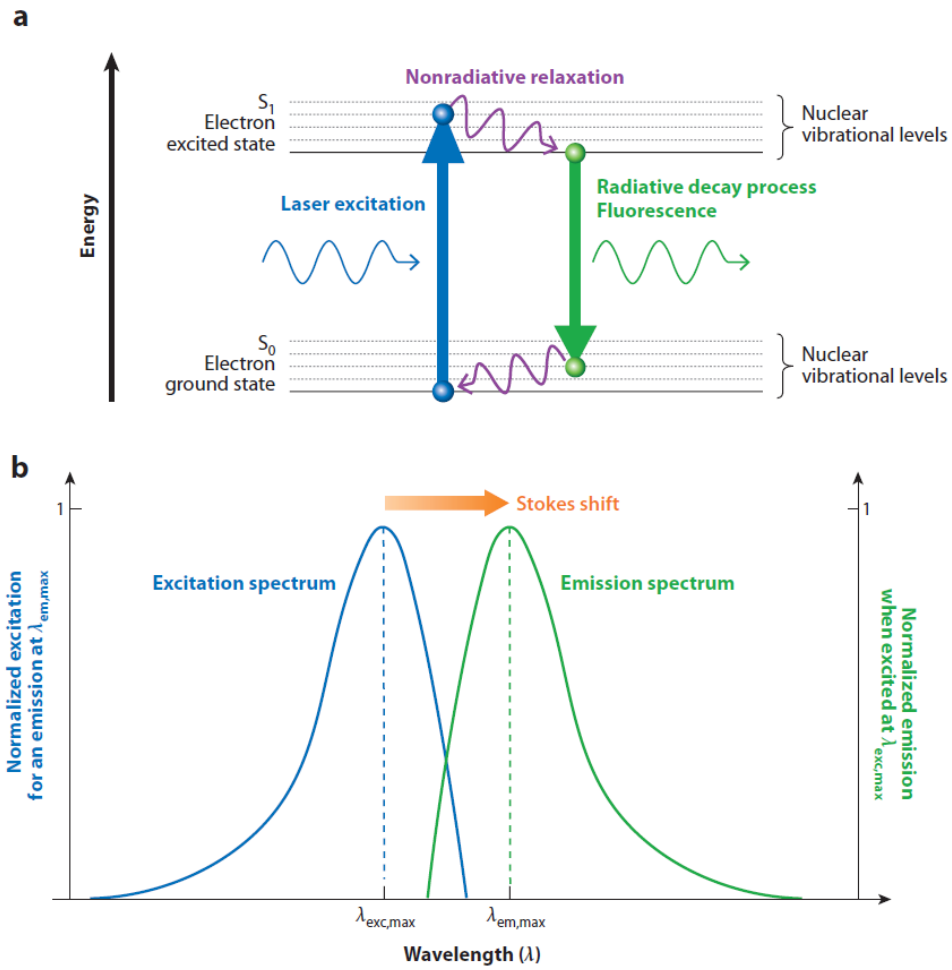

Figure 2.3: The fluorescence process. (a) Simplified Jablonski diagram. (b) Normalized excitation and emission spectra. [11]

with a particle. This concept gave birth to the electron microscopy. Increasing numerical aperture was another way which is successfully exploited in 4-pi confocal microscopy. It is worth mentioning here that one can't make N.A. infinitely large due to practical reasons. In 1994, Stephan W. Hell and Jan Wichmann proposed a technique called stimulated-emission-depletion (STED) fluorescence microscopy breaking down the resolution limit. Theoretically, the resolution limit of STED was shown to be infinite[12]. Many other techniques followed soon after e.g. Structured Illumination Microscopy (SIM), Single molecule localisation microscopy techniques like STORM, PALM etc.

2.2 Fluorescence

Fluorescence plays a crucial role in modern microscopy. Specific targets can be labelled inside the cell which will be visible with high contrast in front of a dark background. Upon shining light of a particular wavelength higher than the energy gap on a fluorescent molecule, the photon might be absorbed and an electron in the ground state is excited to a higher state. This electron then makes a transition to the bottom of the excited energy state through vibrational relaxation. Then it decays back to the ground state emitting a photon which is known as fluorescence (*Fig2.3a*). Due to the non radiative energy loss through vibrational relaxation, the emission wavelength is generally higher than the absorption wavelength. The difference between the maxima of emission and absorption spectra is known as the Stokes shift (*Fig2.3b*).

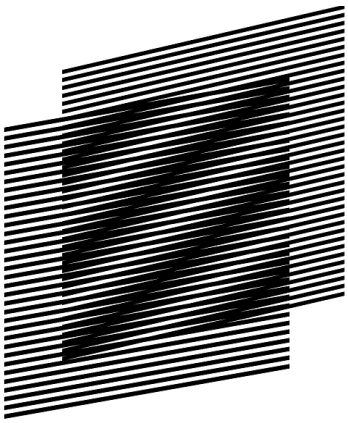

Figure 2.4: Moire effect. Two patterns are overlaid, coarser pattern appears in the middle of two patterns. [13]

While imaging, a filter is placed on the detection arm of the microscope, which only allows the emitted light to pass through. This enables us to image the biological samples with high specificity and contrast. There are many ways for fluorescent labeling the samples. Most commonly used are green fluorescent proteins (GFPs), organic dyes and fluorophores tagged with antibodies.

2.3 Structured illumination microscopy (SIM)

The structured illumination microscope is considered to be one of the best choices for live cell imaging at extended resolution. SIM requires low illumination intensities as compared to most of the other superresolution techniques, uses conventional fluorophores and capture images at wide field of view. Some of the other superresolution techniques (e.g. dSTORM, STED, etc.) can achieve better spatial resolution than SIM, but SIM has advantage of high temporal resolution for large field of view. STED is point scanning technique, it can provide high temporal resolution for a small field of view, while for a bigger field of view STED gives a slow temporal resolution. Single molecule localization techniques are usually very slow, as several thousand images are acquired to generate a single super-resolved image.

SIM makes use of Moiré pattern (*Fig2.4*) to increase the resolution of the fluorescence microscopy. When two fine patterns are overlaid on each other, a coarser pattern appears. In SIM, the sample containing finer details is illuminated with pattern generated by the interference of coherent beams (*Fig2.5*). A third coarser pattern is formed in the light distribution by the sample. The illumination pattern is known and the coarse pattern is detected by the detector. By recording the resulting pattern at different angles, one can deduce the finer details of the sample, thus increasing the resolution of the microscope. Following section gives mathematical details of the image formation and resolution enhancement in SIM.

2.3.1 Mathematical derivation of image generation in SIM

As discussed in *Sec2.1.1*, the OTF puts a limit on spacial frequencies which will be allowed to pass through the system. If $\tilde{F}[A]$ is the object function in frequency space, then this function will be modified after passing through the optical system. Image formed in frequency space will be given by:

$$\tilde{F'}[A] = \tilde{F}[A].OTF \tag{2.3}$$

In real space, image formation can be described as the inverse Fourier transform of eq(2.3). Multiplication in frequency space is convolution in real space, so the imaging process in wide

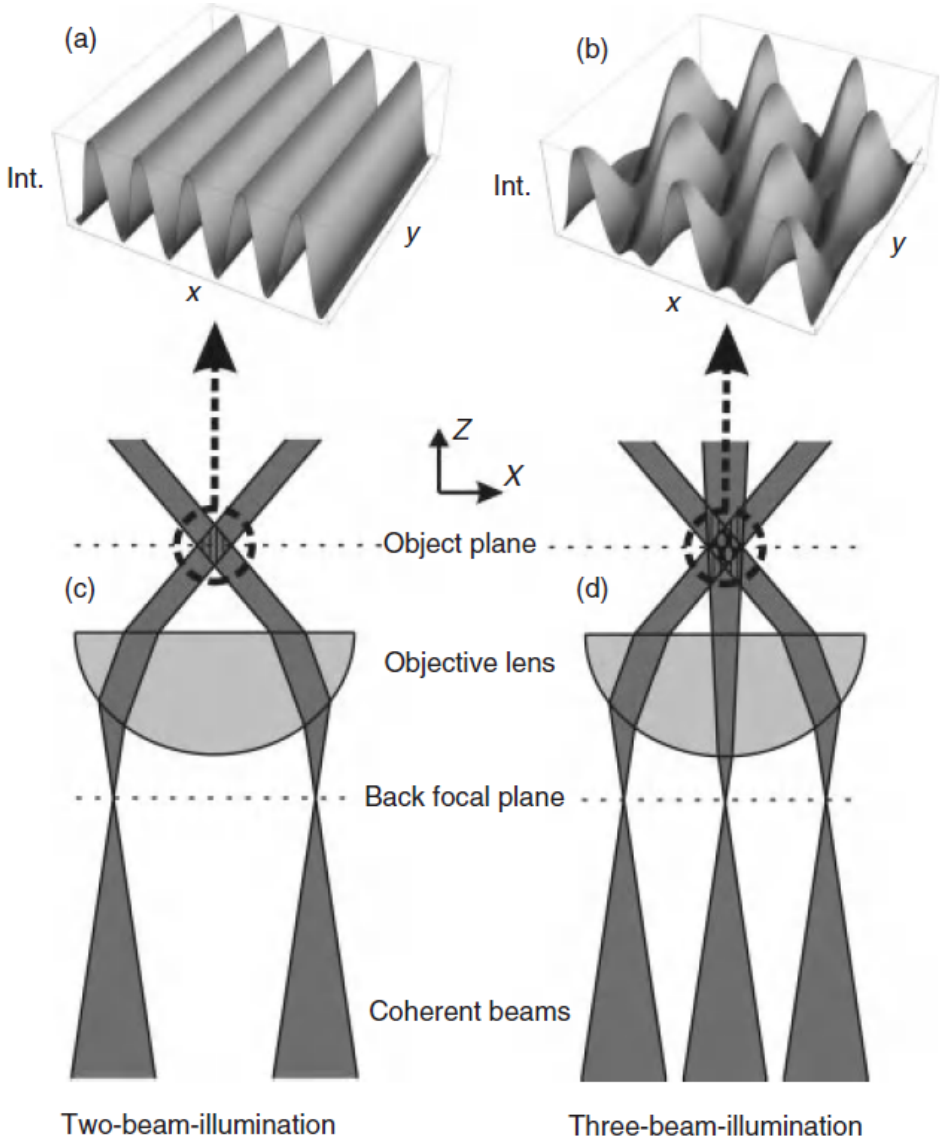

Figure 2.5: Illumination pattern in SIM. In case of 2-D SIM, the interference pattern is produced by the interference of two coherent beams which will increase the lateral resolution twice, as the pattern is varying only along x-direction. In 3-D SIM, the illumination pattern is produced by the interference of three coherent beams. The pattern also varies along z-direction, thus increasing the resolution twice along the depth of sample as well. [14]

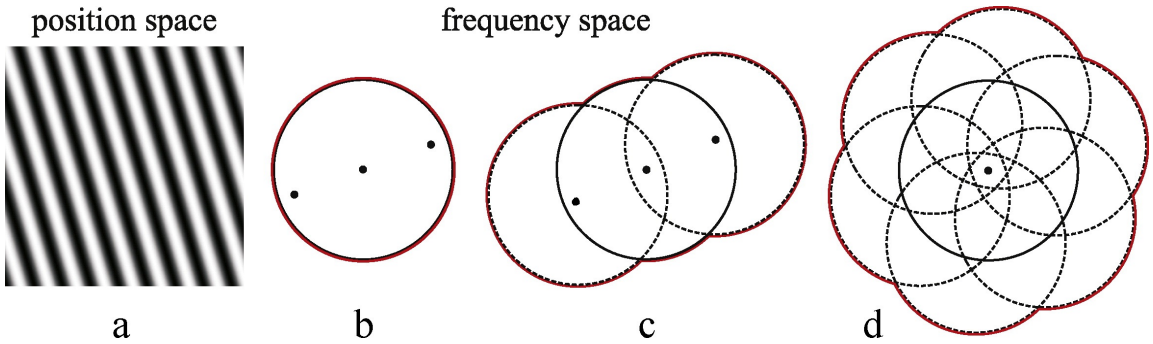

Figure 2.6: Extension of effective OTF in SIM. (a) Sinusoidal pattern illumining the sample in position space. (b) Sinusoidal pattern in frequency space will be three delta peaks. (c) Multiplying OTF with these peaks will increase the effective OTF support and the red boundary shows new cutoff for maximum spacial frequency permitted through the microscope. (c) To achieve isotropic resolution extension, the pattern is rotated.[15]

field microscopy can be described as:

$$A'(\vec{r}) = A(\vec{r}) \otimes PSF(\vec{r}) \tag{2.4}$$

where A is the object function, $\otimes$ is convolution operation and A' is an image of the object. In fluorescence microscopy, the object distribution is proportional to illumination intensity I_{ill} and fluorophore distribution $\rho(\vec{r})$ can be written as:

$$A(\vec{r}) = \rho(\vec{r}) I_{ill} \tag{2.5}$$

In SIM, the sample is illuminated with sinusoidal field and the corresponding intensity can be written as:

$$I_{ill}(\vec{r}) = I_0[1 + m(cos(\vec{k}_G.\vec{r} + \phi))] \equiv I_0[1 + \frac{m}{2}(e^{i(\vec{k}_G.\vec{r}+\phi)} + e^{-i(\vec{k}_G.\vec{r}+\phi)})] \tag{2.6}$$

here m is modulation factor, $\vec{K}_G$ is the spacial frequency of the sinusoidal fringe illumination pattern whose magnitude is $K_G = \frac{2\pi}{G_{SIM}}$ and G_{SIM} is the period of the illumination. ϕ determines the lateral position of the pattern.
In the Fourier space, image formation can be described as:

$$\tilde{A}(\vec{k}) = [\tilde{\rho}(\vec{k}) \otimes \tilde{I}_{ill}] \times OTF(\vec{k}) \tag{2.7}$$

The Fourier transform of illumination intensity can be derived by taking Fourier transform of eq(2.6) and is given by:

$$\tilde{I}_{ill} = I_0[\delta(\vec{k}) + \frac{m}{2} e^{i\phi} \delta(\vec{k} - \vec{k_G}) + \frac{m}{2} e^{-i\phi} \delta(\vec{k} + \vec{k_G})] \tag{2.8}$$

Putting in the value of $\tilde{I}_{ill}$ from eq(2.8) into eq(2.7) and solving, one arrives at the following result:

$$\tilde{A}(\vec{k}) = I_0[\tilde{\rho}(\vec{k}) + \frac{m}{2} e^{i\phi} \tilde{\rho}(\vec{k} - \vec{k_G}) + \frac{m}{2} e^{-i\phi} \tilde{\rho}(\vec{k} + \vec{k_G})] \times OTF(\vec{k}) \tag{2.9}$$

for a conventional uniform illumination, only $\tilde{\rho}(\vec{k})$ contributes but in the case of structured illumination, there are two extra terms positioned at $\vec{k}_G$ and $-\vec{k}_G$. Upon multiplying the OTF with these three terms, the effective OTF of the system increases, thus increasing the cutoff frequency limit. The raw image will be an overlap of the these three frequency spectra, so the information needs to be separated out, then shifted to their respective position in the frequency space. This process is done computationally. The sample is illuminated with (atleast)

three different phase shifted (ϕ_1, ϕ_2, ϕ_3) illumination patterns. This will give us three different frequency spectrum images $\tilde{A}(\vec{k})$. Having this information, the eq(2.9) can be solved to get an information about spectral terms $\tilde{\rho}(\vec{k})$, $\tilde{\rho}(\vec{k} - \vec{k_G})$ and $\tilde{\rho}(\vec{k} + \vec{k_G})$ which consist of separated frequency spectra of the sample. This high frequency spectrum is then shifted to get an extended frequency spectrum of the sample. Taking its Fourier transform yields super-resolved image.[14]

The factor of resolution enhancement depends on $\vec{k_G}$, spacial frequency of the illumination fringes. The sinusoidal pattern is produced by the interference of two plane waves, the maximum spacial frequency that can be produced is, $\vec{k_G} = \frac{2NA}{\lambda_{ex}}$, where λ_{ex} is the wavelength of incident light. Maximum cut-off frequency of the OTF with plane illumination is given by $\vec{k_0} = \frac{2NA}{\lambda_{em}}$, where $\lambda_{em} \approx \lambda_{ex}$ is the emission wavelength from fluorophore. The reconstructed frequency spectrum has a cut-off at $\vec{k_G} + \vec{k_0}$. Hence, the maximum detectable frequency of an object will be:

$$\vec{k}_{SIM} = \frac{4NA}{\lambda_{em}} \tag{2.10}$$

Hence, SIM enhances resolution limit approximately by the factor of 2.

2.4 An overview of some other superresolution techniques

2.4.1 Single molecule localisation microscopy (SMLM)

Working principle of SMLM techniques (e.g. dSTORM, PALM, etc.) is illustrated in *Fig2.7*. In these techniques, the information is separated temporally rather than spatially. Capturing image of a single fluorescent molecule through a conventional microscope will be a spot much bigger than the size of molecules. But, it is possible to localise this molecule with high precision by finding the centroid of the resultant PSF. Photo-switchable fluorophores are used to stain the cell, such that, only a few molecules lying at a distance greater than the diffraction limit from each other at a given instant are emitting the signal. At next time-frame (generally the difference between each time-frame is few ms), these molecules are shut down and different molecules are in on-state (emitting signal). Several thousand images are captured at different time-frames and combined to get a final image. Resolution of an image will depend on how precisely our molecule is localised. This localisation precision of a molecule [17] is given by:

$$\sigma = \sqrt{\left(\frac{s^2 + \frac{a^2}{12}}{N}\right).\left(\frac{16}{9} + \frac{4\pi s^2 b^2}{a^2 N}\right)} \tag{2.11}$$

N is the no. of photons collected from each fluorescent molecule, s is the standard deviation of the PSF, a is the pixel size, b is the background noise level. Here N is one of the most important factors which decide the resolution of our image. Larger N means more localisation precision and more signal to noise ratio. The resolution also depends on labelling density. The labeling density should be twice as high as desired resolution following the Nyquist-Shannon theorem and the size of labelling should be as low as possible. Tens of thousands of snapshots of a particular sample are taken and then a two dimensional Gaussian curve is fitted to each possible point of fluorescent molecules. The FWHM of this curve is determined by eq(2.11) and the amplitude is proportional to the value of N (*Fig2.7*). Then all these Gaussian fitted snapshots are combined to get final super-resolved image [19].

2.4.2 Stimulated emission depletion (STED) microscopy

In STED, the sample is made to emit the fluorescence signal from an area shorter than the diffraction limit. This kind of illumination is achieved by using two laser beams, one to get fluorescence and another to produce a donut shaped beam that depletes (by stimulated emission)

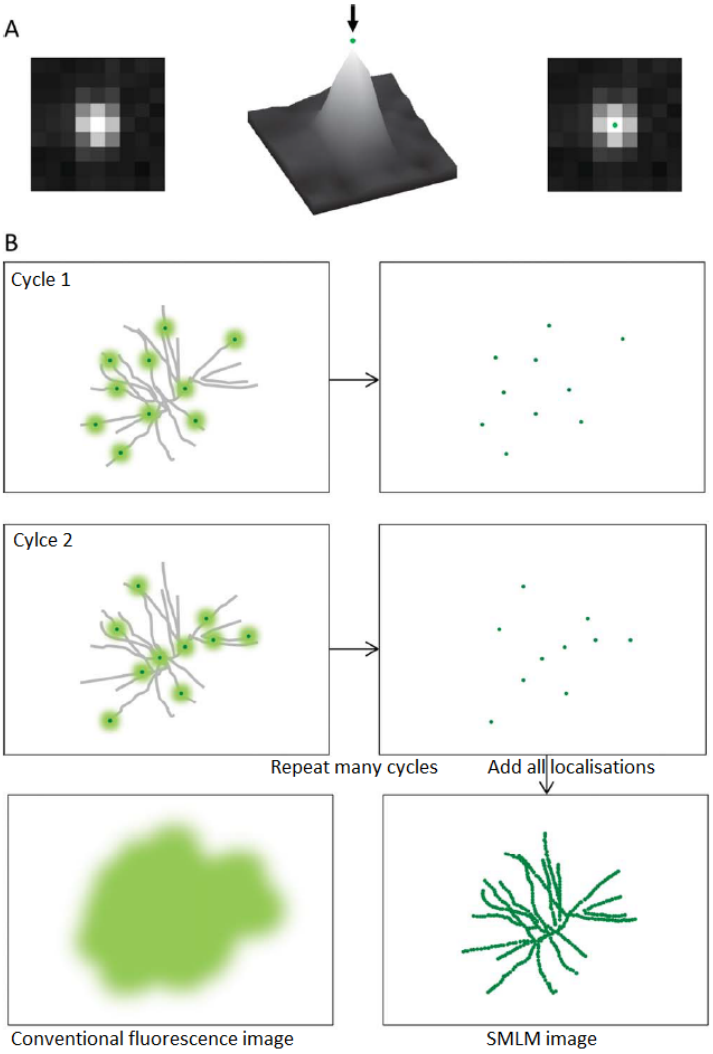

Figure 2.7: Principle of SMLM in nutshell: (a) Image taken by camera of a singe molecule and its localisation (green dot). (b) At a single instant, few fluorophores lying at a distance greater than diffraction limit are emitting. An image is taken and the molecules are localised. Then this process is repeated for thousands of time and finally all the localisations are localised to get a super-resolved image.[18]

the fluorophores in the excited state, except the fluorophores in the center of the beam (*Fig2.8*). Then the sample is scanned-through to get whole image of the sample. FWHM of effective fluorescence area for STED is given by:

$$r = \frac{\lambda}{2nsin(\alpha)\sqrt{1 + \frac{I_{max}}{I_{sat}}}} \tag{2.12}$$

where $I_{sat} = 1/(\tau_{fl}\sigma)$ is the saturation intensity of fluorescence of at which its value is reduced to $1/e$ of its maximum value. τ_{fl} is the lifetime of the excited state and σ is the transition cross section of STED laser wavelength I_{max} is the depletion intensity[21]. Typically, $I_{sat} = 10MW/cm$ and $I_{max} = 100MW/cm$ [20]. Increasing the value of I_{max} arbitrarily large resolution can be achieved. Hence its resolution can be infinite, theoretically. Though, one cannot just arbitrarily shine high laser intensity on a sample as biological sample can be destroyed. The wavelength of STED laser is longer than Excitation laser to avoid secondary excitation of fluorophores. By using STED, one can achieve resolution as low as $20nm$. Due to very high power, sample can photobleach very fast, hence live cell imaging is hard performed. Special

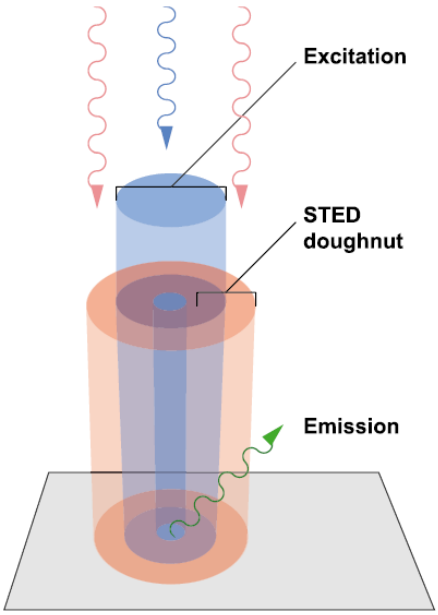

Figure 2.8: Bear profile of STED laser. Fluorescence is emitted from a very narrow area.[20]

fluorophores are also needed for labeling biological sample.

2.5 Quantitative phase microscopy (QPM)

Most of the biological samples, e.g. cells are transparent and thus contrast of the image is very poor in the bright field image. Phase contrast microscope provides better contrast and reveals finer structures through visualisation, though, one can't quantify the variations in the phase. The phase variations are directly related to the biophysical parameters, such as, thickness and local refractive index variations in the sample. Phase variations are quantified using quantitative phase imaging (QPI) techniques. (*Fig2.9*) shows typical quantitative phase contrast image of the cells in culture. The advantage of using QPI is that it does not require any labelling and the phase information can be extracted from the single recorded intensity pattern, thus preventing phototoxicity. In this section, I will just explain the basic principle of QPI. The rigorous theoretical description is out of the scope of my thesis.

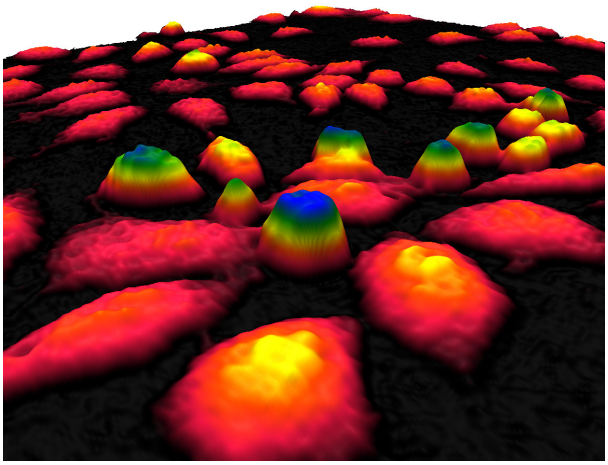

Figure 2.9: Quantitative phase image of cells in culture. The height and color of an image point correspond to the optical thickness, which only depends on the object's thickness and the relative refractive index.[22]

Upon illuminating an object under the microscope with a plane wave, the intensity $O_0(x, y)$ and phase $\phi(x, y)$ of the transmitted light at the image plane will vary due to transmittance variations in the object. Transmitted wave at an image plane can be represented as:

$$O_i(x, y, t) = O_0(x, y)e^{-i(\vec{k}.\vec{r}-\omega t+\phi(x,y))} \tag{2.13}$$

But only the intensity is recorded by the detector, which is the modulus square of the field, $|O_0(x, y)|^2$. Thus the phase information is lost and one can only see the amplitude variation at image plane. The trick to recover the phase information is by mixing the image field with another plane wave known as reference field,

$$R_i(x, y, t) = R_0(x, y)e^{-i(\vec{k_R}.\vec{r}-\omega t_R)} \tag{2.14}$$

For brevity, I will denote the amplitudes $O_0(x, y) = O_0$ and $R_0(x, y) = R_0$ in further calculations. The resultant intensity at the image plane after interference of both fields is given by:

$$\begin{aligned} I(x, y, t) &= |O_i(x, y, t) + R_i(x, y, t)|^2 \\ &= |O_0|^2 + |R_0|^2 + O_i^*(x, y, t)R_i(x, y, t) + O_i(x, y, t)R_i^*(x, y, t) \\ &= |O_0|^2 + |R_0|^2 + 2|O_0||R_0|cos[\omega(t - t_R) - (\vec{k} - \vec{k_R}).\vec{r} + \phi(x, y)] \end{aligned} \tag{2.15}$$

The resulting intensity contains information about the quantity of interest, $\phi(x, y)$, which can be extracted using various QPI techniques such as phase shifting method, off-axis method, etc.

2.6 The placenta and its function

The placenta is an interfase tissue joining the mother and the fetus, which allows the passage of nutrients and oxygen from mother to the fetus. It also permits the release of waste from the fetus back into mother's systemic circulation. After fertilisation, when the embryo reaches a stage known as morula, it begins to differentiate into two groups of cells: outer cell layer called the trophoblast and an inner layer called the inner cell mass. Trophoblast forms the fetal part of the placenta, whereas, the inner cell mass develops into a fetus.

An embryo during the fifth to sixth day after fertilization consists of about a hundred cells in the form of a fluid filled hollow sphere called blastocyst. At the end of the first week, the blastocyst attaches to the endometrium. Soon after the attachment, the trophoblast layer divides into two layers: inner layer called the cytotrophoblast and outer layer called the syncytiotrophoblast. Syncytiotrophoblasts produce certain enzymes, which gradually removes the maternal tissue, as a result, finger like projections of the syncytiotrophoblast extend through the endometrium[23]. The trophoblast cells then invade the spiral arteries in the endometrium in order to set up supply of nutrients to the fetus and this process is known as trophoblast invasion (*Fig2.10*).

Implantation of an embryo and the development of fetus happens in the uterus of a female. The Uterus is a female organ which is connected from one end to the vagina through an opening called cervix and another end connected to both fallopian tubes. It consist of three layers: endometrium, myometrium and serosa. Endometrium is lining of the uterus made up of epithelial cells. During the pregnancy, the endometrium layer becomes thicker and the number of blood vessels present in it increases in size and number. After implantation, the endometrium in a pregnant woman is known as decidua or decidua basalis. Decidua forms the maternal part connecting placenta (*Fig2.11*).

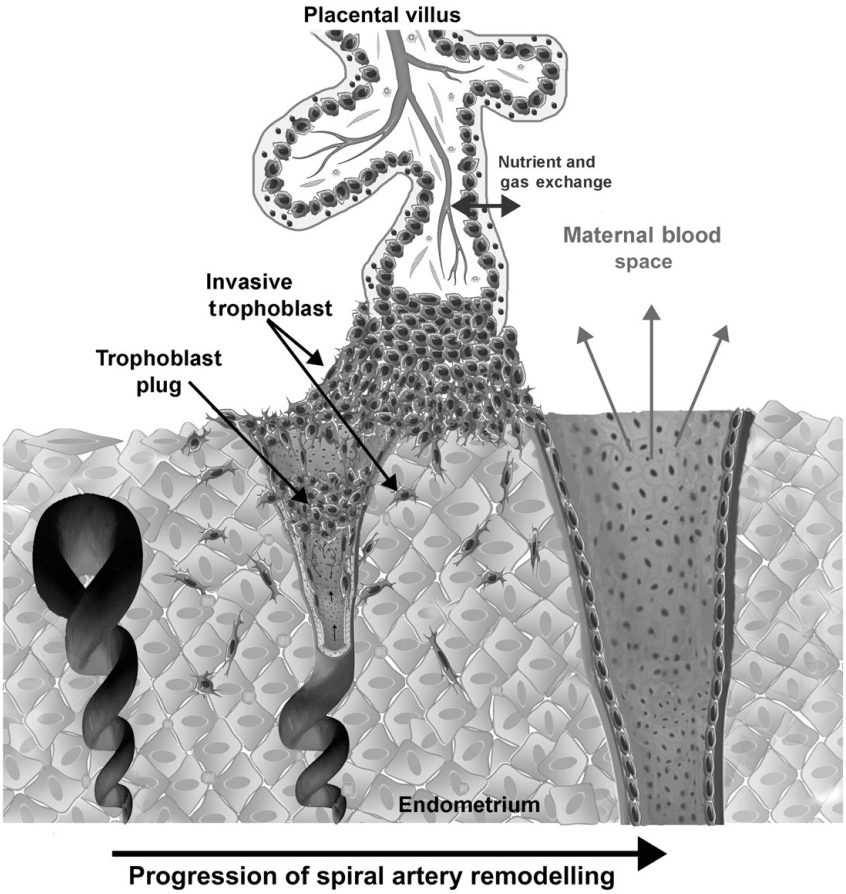

Figure 2.10: Spiral artery remodelling through trophoblast invasion. During first trimester, the trophoblasts accumulate and form a plug in spiral artery which only allow the blood plasma to seep through. Fetus growth occur in low oxygen state resulting in a physiological oxygen gradient between mother and fetus. Between 10-12 weeks, these plugs are dislodged flooding intervillus space with maternal blood. [25]

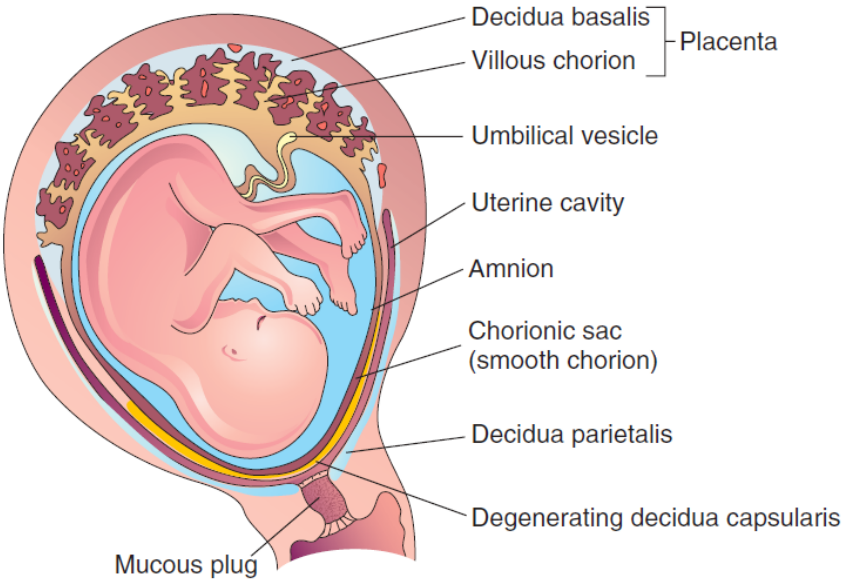

Figure 2.11: Inside the womb: fetus is connected through placenta to mother. Villous chorion is in contact with the maternal blood and allows the passage of nutrients to fetus from mother.[23]

2.7 Trophoblast-macrophage crosstalk at feto-maternal junction

Macrophages play an important role in immune response, tissue development, remodelling and repair, etc. They are generally classified into two categories depending on how they respond to the various environmental signals: classically activated macrophages (M1) and alternatively activated macrophages (M2). M1 macrophages are stimulated by the virus infections, endotoxin (LPS) or some cytokines e.g. TNF-α, INF-γ, etc. which maximises their cytotoxic and inflammatory capabilities. Important cytokines, such as IL-1, IL-6, IL-12 and TNF-α are released in response. M2 macrophages help in the tissue remodelling and repair and are characterised by the release of the cytokines such as IL-2β and IL-10.[5]

The presence of the macrophages at implantation site can be explained as the response of maternal body to the paternal antigens. Studies have shown that initially, the trophoblasts release monocytes attractants which promotes their migration towards decidua, surrounding the trophoblast cells. Then these monocytes differentiate into the macrophages. Decidua in a pregnant woman contains $20-30\%$ macrophages of the total population of the leukocytes. During peri-implantation period, the decidual macrophages are inclined towards M1 phenotype. Their profile predominantly shifts towards M2 macrophage phenotypes during the pregnancy. Macrophages play important role in the spiral artery remodelling and the trophoblast invasion by clearing the apoptotic cells in the decidua.[24] For a successful pregnancy, balance between M1 and M2 polarisation of macrophages is important during the gestation period.

Factors such as infections, inflammatory diseases or aberrant classical activation of macrophages may disturb the normal macrophage function and lead to various pregnancy complications. Classically activated macrophages produce TNF-α and nitric oxide (NO) in abundance which has been linked with pre-eclampsia, preterm delivery and early abortion. *Fig2.10* shows systematic diagram of macrophage-trophoblast molecular cross-talk during normal and pathological pregnancy. TNF-α may also be capable of inducing apoptosis in the trophoblast cells.[24] Some studies suggest that first trimester trophoblast cells have the capability to keep pro-inflammatory cytokines under control by interacting with macrophages, if the dose of LPS is low ($0.1\mu g/ml$). They were unable to suppress them in the case of high dose ($10\mu g/ml$) of

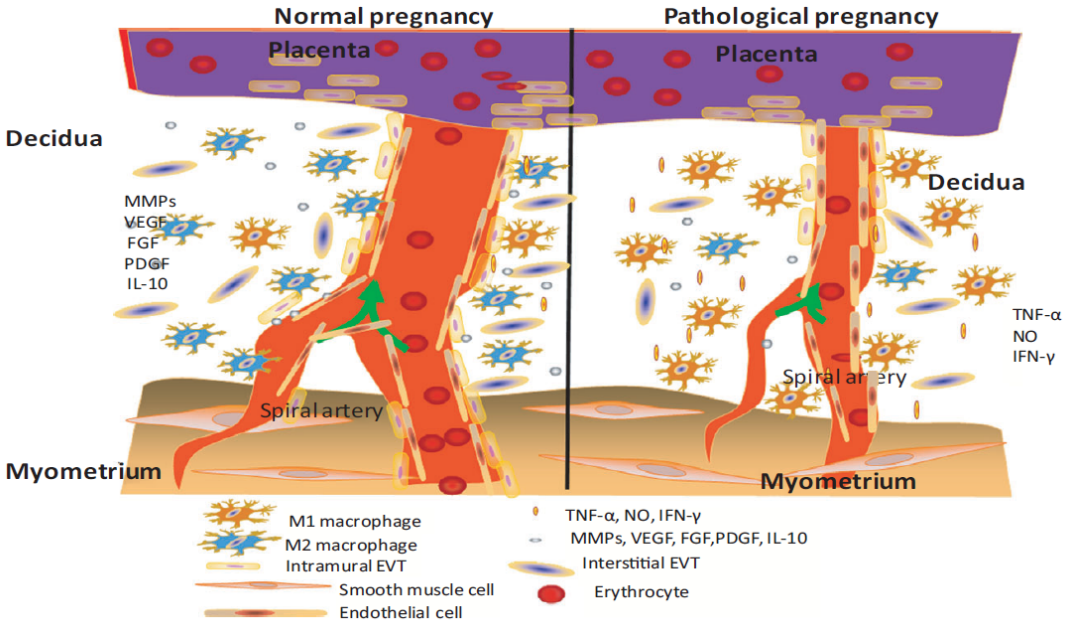

Figure 2.12: Systematic diagram showing macrophage-trophoblast molecular cross-talk during normal and pathological pregnancy. During normal pregnancy, various factors such as vascular endothelial growth factor (VEGF), fibroblast growth factor (FGF), IL-10, etc. are produced which are important for spiral artery remodeling, trophoblast invasion, phagocytosis, etc. In contrary, during pathological pregnancy, increased number of M1 macrophages produce pro-inflammatory factors which can disturb the fetal growth.[5]

LPS. Generally, the level of nitrates and nitrites, which are the metabolites of NO are elevated in the case of the pre-eclamptic women.[39]

Chapter 3

Measurment of nitric oxide in stimulated macrophages and trophoblasts

"There are very few things in our body that nitric oxide doesn't regulate." ~ Dr. Ferid Murad

3.1 Introduction

Both macrophages and trophoblasts are able to produce nitric oxide. Different studies attribute different roles to nitric oxide produced by these cells in the process of embryonic implantation during pregnancy. Previous studies have shown that the nitric oxide produced by trophoblast may play a role in the successful outcome of the implantation by dilating uteroplacental arteries, while nitric oxide produced by macrophages plays a role in the regulation and apoptosis of trophoblasts.[26] Overproduction of NO by macrophages can have a negative effect on the pregnancy.[5]

Nitric oxide is an unstable free radical and thus reacts with oxygen instantly to form nitrites (NO_2^-) and nitrates (NO_3^-). We measured the nitrite levels present in the cell culture media, which are directly proportional to the amount of nitric oxide produced by the cells.[27] Thus measuring nitrite levels indirectly gives us the amount of NO produced. Both cell lines were cultured by using the same type of media, induced by the same concentration of inflammatory agents, and the amount of nitrite was measured in a similar fashion. NO was measured at $0hr$, $4hr$, $8hr$, $12hr$, $24hr$ time points for both cell lines after challenge with one of the three different inflammation inducing agents at different concentrations as shown in table 3.1. In literature, researchers have used various concentrations of LPS varying from $50pg/ml$ to few $10\mu g/ml$, in vitro.[28, 29] Typically, in preeclamptic placenta, the levels of TNF-α are found to be around $200pg/ml$.[30]. Some protocols suggest that $5\mu g/ml$ concentration is enough to stimulate T-cells.[31] Our decision of choosing concentrations was based on these studies and the discussions with clinical practitioners. The Griess test is done to detect the amount of nitrite ions in the solution. The solution turns pink in the presence of nitrites when mixed with Griess reagent. Nitrite levels were measured quantitatively in μM by comparing the absorbance of the test sample with that of a standard sample of sodium nitrite ($NaNO_2$). The Griess reagent is easy to prepare and is cheaper to perform as compared to other NO measurement methods, but the lower limit of detection for Griess testing is just $1\mu M$.[27]

LPS	TNF-α	Con-A
$100ng/ml$	$10pg/ml$	$100ng/ml$
$1\mu g/ml$	$100pg/ml$	$1\mu g/ml$
$10\mu g/ml$	$1ng/ml$	$10\mu g/ml$

Table 3.1: Inflammation inducing agents and their concentrations used in the experiments

3.2 Experimental methods

3.2.1 Materials and instruments

RPMI 1640 ($\#R8758$), LPS ($\#L2880$), TNF-α ($\#T5944$), Concanavalin-A ($\#C2272$), sulphanilamide ($\#S9251$), naphthalene diamine dihydrochloride ($\#N91250$) and Dulbecco's PBS ($\#D8537$) were bought from Sigma-Aldrich, St Louis, MO, USA. Agilent 8453 UV-Visible Spectrophotometer, Agilent Technologies, Santa Clara, USA. FALCON 24-Well cell culture plates, Corning Incorporated, New York, USA. Zeiss standard binocular microscope, Carl Zeiss, West Germany with 10X and 40X objective lenses.

3.2.2 Cell lines and cell culture

RAW 264.7 and HTR-8/SVneo cell lines analysed in the experiments were from ATCC and were collected from the Laboratory of Women's Health and Perinatology at UiT. RAW 264.7 cells are murine (mouse) macrophages, immortalised by inducing Abelson murine leukemia virus. HTR-8/SVneo cell line was derived in 1992 by immortalizing the trophoblast cells that grew out of chorionic villi of human first-trimester placenta. Both cell lines adhere to the surface during culture.

Both cell lines were cultured separately in a humidified atmosphere of 95% air and 5% CO_2 at 37^0C with glutamine containing RPMI-1640 medium supplemented with 10% fetal bovine serum and antibiotics (penicillin and streptomycin). The cells were subcultured every 2-3 days by transferring about 20% of the cells to the next passage (transferring some amount of cells to new flask) and were utilised for experiments at $80-90\%$ confluency.

3.2.3 The Griess method for NO measurement

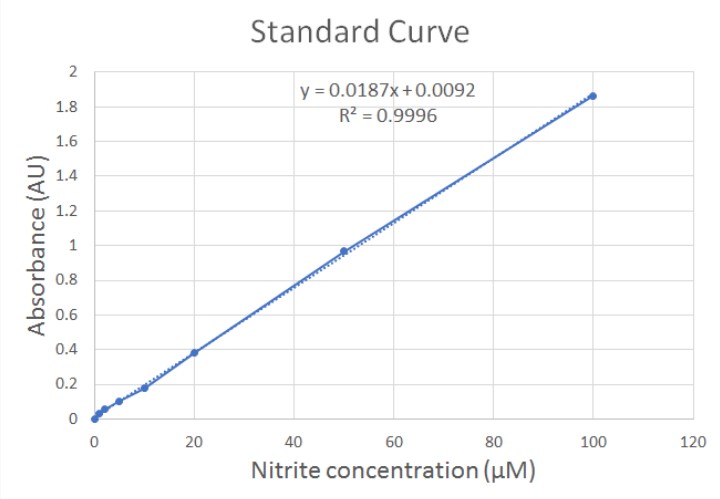

Figure 3.1: Standard curve is linear and is used to quantify the concentration to nitrites present in the culture media.

Preparation of Griess reagent:

Griess reagent is prepared by adding 2.5% solution of phosphoric acid in distilled water. 1% sulphanilamide and 0.1% naphthalene diamine dihydrochloride are added to that solution and mixed well. The reagent is then protected from the direct light exposure. The protocol to prepare the standard curve is:

1. Standard solutions of sodium nitrite ($NaNO_2$) were prepared with following concentrations: $0\mu M$, $1\mu M$, $2\mu M$, $5\mu M$, $10\mu M$, $20\mu M$, $50\mu M$, $100\mu M$, $200\mu M$.
2. Griess reagent ($300\mu l$) was mixed with standard solution of each concentration of $NaNO_2$ described in step 1.
3. Each solution from step 2 was individually transfer into the cuvette and absorbance on a UV spectrometer was measured corresponding to the wavelength $540nm$.
4. For each concenration, three independent experiments were conducted.
5. A curve for concentration vs. absorbance was plotted (*Fig3.1*).

Quantisation of NO levels:

A standard curve (*Fig3.1*) is prepared to quantify the unknown nitrite concentration in any solution. Once a standard curve is prepared, absorbance from the culture media is measured at $540nm$ on UV spectrometer. Then this value of absorbance is compared with standard curve and a corresponding concentration of nitrite is calculated using the linear equation. The absorbance of an unknown sample (x) is measured on UV spectrometer corresponding to 540 nm. The nitrite concentration (y) from this curve can be calculated as follows: $y = \frac{x-0.0092}{0.0187}$

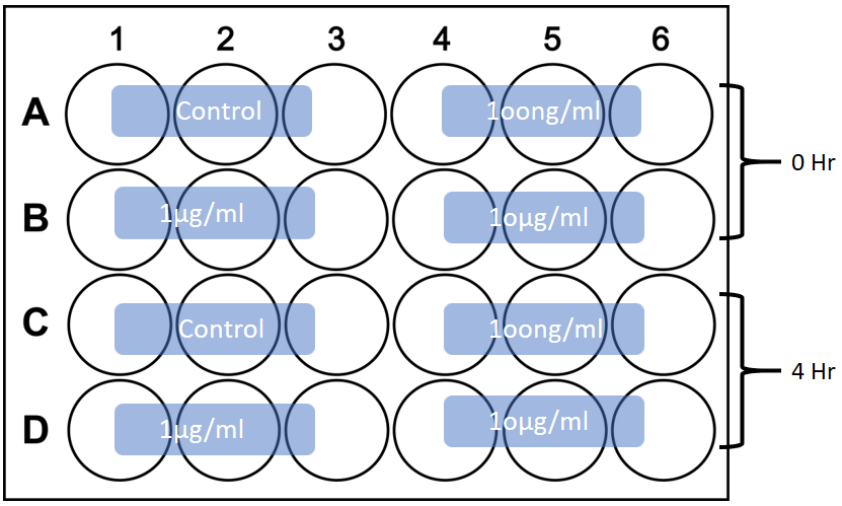

Figure 3.2: Representative 24-well plates of nitrite assays. This figure represent the plan for LPS-challenged cells in which nitrite concentration will be quantified after $0hr$ and $4hr$. Similar plates were prepared for $8hr$, $12hr$ and $24hr$ studies. Same method was adopted for other two inflammation inducing agents as well.

Measurement of NO in cell culture media:

For the nitrite measurement, 1×10^5 cells/ml were transferred to each well of the 24-well plates. The cells were allowed to stabilize and adhere for 24 h in an incubator at 37^0C and 5% CO_2. The inflammation-inducing agents were added to these wells afterwards, according to the following procedure:

Each plate was divided into two sets (12 wells each). Each set was further divided into a subset of 3 wells. One subset was kept as a control and the other three subsets were challenged with three different concentrations of a particular inflammation-inducing agent as shown in (*Fig3.2*).

3.3 Results and discussion

3.3.1 LPS induces NO production in macrophages, but not in trophoblasts

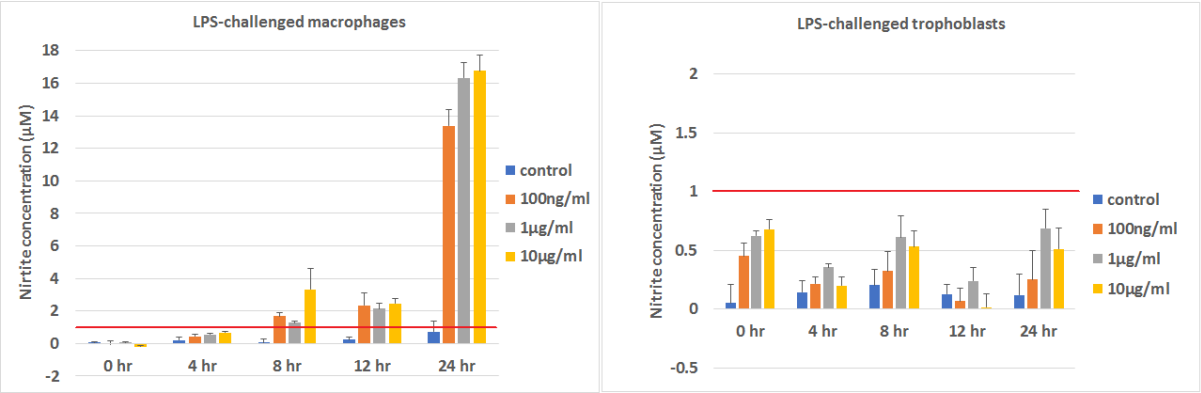

Figure 3.3: The production of NO by macrophages (left) and trophoblasts (right) following LPS-challenge at various concentrations. Bar graph shows the mean value (+S.D.) of three experiments. Considerable amount of NO was produced only in case of macrophages stimulated by LPS. (The horizontal red line shows the detection limit for NO measurements.)

LPS is an endotoxin known to induce cellular stress in response to which some cells, e.g. macrophages produce NO. We measured the response of macrophages and trophoblasts upon challenging them with various concentrations ($100ng/ml$, $1\mu g/ml$, $10\mu g/ml$) and at different time points ($0hr$, $4hr$, $8hr$, $12hr$, $24hr$). Upon activation of macrophages with LPS, large amount of NO is produced after $24hr$. From *Fig3.3*, it can be seen that compared with control, challenged cells already started producing NO, but they are below the lower detection limit of Griess method, so the results after $4hr$ are not conclusive. After $8hr$, UV spectrometer started detecting the nitrites and the nitrite concentration remains almost constant until $12hr$. The maximum increase in the NO production is seen between $12 - 24hr$. An increase in the NO production was expected and is in accordance with the previous studies.[32, 33]

In contrast, trophoblasts were not able to produce any significant increase in the amount of NO even after $24hr$ following LPS-challenge. A possible reason for this might be that the iNOS-enzyme is not as active as in trophoblasts as compared with macrophages. Another reasons might be that the concentration of LPS was not enough to induce the effect or the time frame for the stimulation was not enough. Some studies suggest that primary trophoblasts produced a significant amount of NO with $100\mu g/ml$ LPS after $24hr$.[34]

Upon comparison of the results between macrophages and trophoblasts, one can infer that similar inflammatory conditions result in different amounts of NO production. It is worth mentioning here that both cell types have toll like receptors (TLR-4) which recognises the LPS. Macrophages produce significant amounts of NO upon activation by LPS, but trophoblasts failed to produce a significantly higher amount of NO. We repeated the experiment three times and every time similar results were obtained. The negative values in the results are due to blank error.

3.3.2 TNF-α induces NO production in neither macrophages nor trophoblasts

TNF-α is released by macrophages upon stimulation of LPS. During the first trimester, it may be involved in the regulation of trophoblast differentiation.[5] Some studies suggest that the TNF-α was elevated in case of pre-eclamptic placenta.[24] Macrophages and trophoblasts were challenged with different concentrations of TNF-α ($10pg/ml$, $100pg/ml$, $1ng/ml$) and measured the corresponding nitrite concentration in the cell culture media.

Both macrophages and trophoblasts do not show significantly increased levels of NO production even after $24hr$ of stimulation, which can be seen in *Fig3.4*. Some values are above the detection limit, but the standard deviation for these readings is also large. Our results suggest that though, TNF-α is produced by the macrophages after classical activation, but it might not stimulate the macrophages directly to produce NO. According to [35, 36], macrophages are activated by TNF-α in combination with interferon gamma (INF-γ). So far, we have not come across any literature discussing NO production by trophoblasts after TNF-α challenge. Our results suggest that TNF-α might not induce nitric oxide synthase in case of trophoblasts. Future studies could investigate how trophoblasts behave in combination with TNF-α and INF-γ.

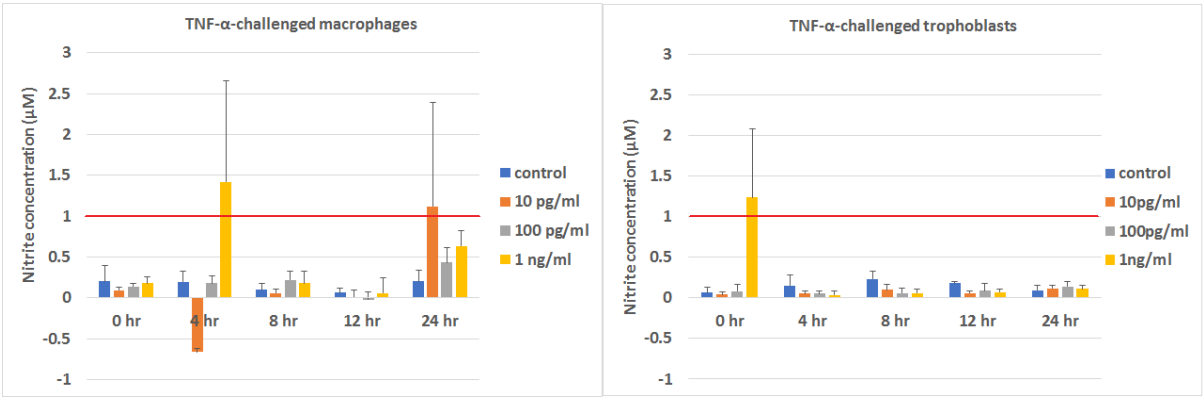

Figure 3.4: The production of NO by macrophages (left) and trophoblasts (right) following TNF-α-challenge at various concentrations. Bar graph shows the mean value (+S.D.) of three experiments. (The horizontal red line shows the detection limit for NO measurements.)

3.3.3 Con-A induces NO production in neither macrophages nor trophoblasts

Concanavalin-A (Con-A) is a plant mitogen, which is known to cause inflammation in some mouse lymphocytes.[37] It is not produced naturally in our body and is not known to cause pregnancy complications. However, we wanted to see how macrophages and trophoblasts would react to such inflammatory agent. Macrophages and trophoblasts were challenged with different concentrations of Con-A ($100ng/ml$, $1\mu g/ml$, $10\mu g/ml$) and corresponding nitrite concentration was measured in the cell culture media. Neither macrophages nor trophoblasts produced significantly increased amount of NO. From *Fig3.5*, one can see that there are some values above the detection limit of the setup, but they might be due to experimental error. There have been some studies on effect of Con-A on different kinds of macrophages, but the nitrites detected were of the order of nM concentration.[38] Our setup is not able to detect these amounts. Moreover, this value might vary according to the cell type. No literature was found on NO production by trophoblasts upon Con-A challenge.

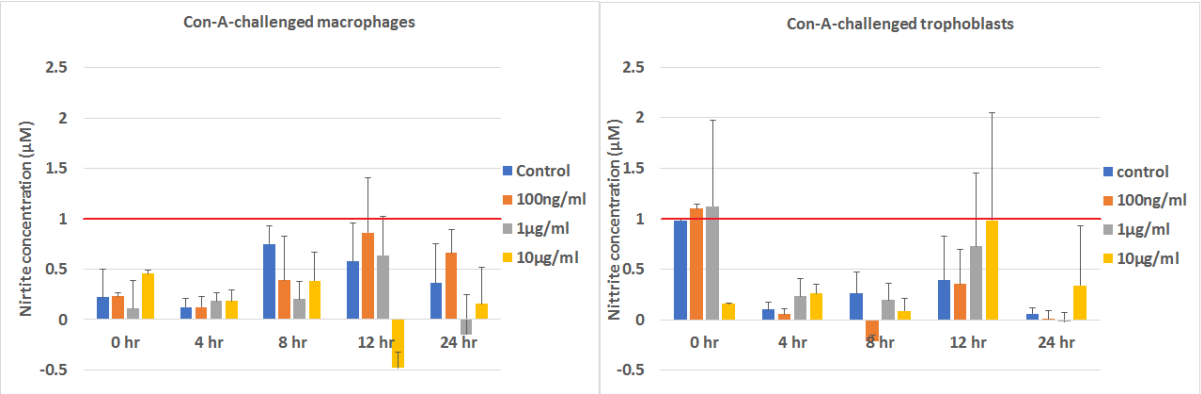

Figure 3.5: The production of NO by macrophages (left) and trophoblasts (right) following Con-A-challenge at various concentrations. Bar graph shows the mean value (+S.D.) of three experiments. (The horizontal red line shows the detection limit for NO measurements.)

Chapter 4

Multimodality imaging of stimulated trophoblasts and macrophages

One thing I liked about being in microscopy is it gets you out of your box constantly because there's such a diverse range of applications. ∼ Dr. Eric Betzig

4.1 Introduction

The Griess reagent has low sensitivity, detecting nitrites $\geq 1\mu M$.[27] NO is not be detected until nitrite levels reach the detection limit of the Griess test. The inflammatory environment might still affect sub-cellular morphology before nitrite levels reach above the detection limit. High resolution microscopy can be used to analyse a single cell at a time and thus can detect the morphological changes at cellular level at an early stage. While SIM provides specific sub-cellular information of mitochondria and plasma membrane, QPM is used to obtain information about the thickness of the cell or the cellular content. Thus, multimodal imaging approach was adopted to study the inflammatory response of macrophages and trophoblasts.

Two sets of experiments were carried out with different aims. The first aim was to see if there are any sub-cellular morphological changes after $24hr$ of inflammatory stimuli. Another set of experiments was carried out to detect how early the sub-cellular morphology start changing after the stimulus. Most of the time during this research project was spent on experiments with $24hr$ incubation time; early time-point experiments were done during the last month of the project period and this work can be further extended.

Mitochondria utilizes oxygen during energy production and reactive oxygen species (ROS) e.g. superoxide ($O_2^{\cdot -}$), hydroxyl radical ($HO^{\cdot}$), alkoxyl radical ($RO^{\cdot}$), etc. are generated as the byproduct. $O_2^{\cdot -}$ may react with NO to produce reactive nitrogen species (RNS) e.g. peroxynitrite ($ONOO-$), which has strong damaging effects on the cell. ROS affect many cellular functions, such as autophagy, anti-microbial effects, cell differentiation, inflammation, etc. ROS also regulates mitochondrial fission and fusion, thus, controlling the overall morphology and function the of mitochondria.[41] Generally, fission and fusion rates are equal, but imbalance in these processes can lead to the alteration of morphology and function of mitochondria. Cells with high fusion-to-fission ratio have fewer number of mitochondria, which are long and highly interconnected. Cells with low fusion-to-fission ratio have higher number of mitochondria, which are shorter and are often referred to as fragmented mitochondria.[42]

Any damage to the mitochondria can cause cell dysfunction and eventually leads to cell death.[43] Thus we investigated the morphological changes in mitochondria in response to inflammatory environment. It can be seen while observing under a simple microscope that the size of macrophages increases after LPS challenge. Through our experiments we also studied plasma membrane morphological changes in macrophages using SIM and QPM. QPM was also used to study the effect of inflammatory stimuli on the phase value of cells, which is related to

their thickness and refractive index of cellular content.

In *Ch3*, three concentrations for each inflammatory agent were used. From *Fig3.3* it can be seen that NO is produced significantly by all three concentrations ($1ng/ml$, $1\mu g/ml$, $10\mu g/ml$) of LPS used after $24hr$. We decided to opt for middle concentration $1\mu g/ml$. TNF-α and Con-A challenge could not induce NO production in macrophages and trophoblasts, it was therefore decided to use the highest concentration (TNF-α: $100ng/ml$ and Con-A: $10\mu g/ml$) for both.

4.2 Experimental methods

4.2.1 Materials and instruments

CellMask Green (CMG) ($\#C37608$), MitoTracker Green (MTG) ($\#M7514$) and live cell imaging solution ($\#A14291DJ$) were bought from Thermo Fisher Scientific (Waltham, USA). #1.5, 25mm round coverslips ($\#631-0172$) were bought from VWR international. Human fibronectin purified from human plasma by affinity chromatography on Gelatin Sepharose 4B was a kind gift from Vascular Biology Research Group, Dept. of Medical Faculty. Commercial OMX 3D-SIM v4 blaze system (GE Healthcare, USA). Quantitative phase microscope is custom build at optical nanoscopy lab, UiT-The Arctic University of Norway.

4.2.2 Sample preparation

The plasma membrane and mitochondria were labelled in our experiments using CellMask Green (CMG) and MitoTracker Green (MTG), respectively. Both dyes are excited by the same wavelength ($\lambda_{ex} = 488nm$). CellMask, is an amphipathic molecule containing a lipophilic part for membrane loading and a negatively charged dye for membrane anchoring.[45] Mitochondria are generally difficult to visualise under phase contrast or differential interference contrast microscopy. Hence, labels play a vital role in the study of mitochondria using microscopy. As mitochondria have negative transmembrane potential, the dyes used, e.g. MitoTracker (green, red etc) to probe them are generally positively charged and lipophylic.[46] However, MitoTracker chemically reacts and link to thiol groups in the mitochondria.[47]

For SIM imaging, cells (cultured as described in section 3.2.1) were seeded on #1.5 coverslips ($170\mu m$ thick) the day before imaging and were incubated. Next day cells were challenged with inflammatory agents. They were labelled and imaged after various time points. For QPM, the cells were seeded on silica chips with a reflecting surface. Before seeding the cells, the surface was treated with fibronectin for 20 minutes. The chips were then washed thrice with PBS and cells were seeded and incubated for $24hr$. Next day cells challenged with inflammatory agents. They were labelled and imaged after various time points.

A fair amount of time during this master research project was spent on optimising the labelling protocols for both cell lines. Different concentrations for MTG were tried ($30-75nM$) for different time periods ($15-45mins$). After a series of experiments, cells incubated with $60nM$ of MTG concentration for $30mins$ was found to be optimum for both the cell lines and further experiments were carried out using these parameters. For CMG, labelling the samples with ratio of stock solution of CMG to RPMI, $1:1000$ for $10mins$ was found to be optimum. Oil #1.1516 (provided along with OMX-setup by GE Healthcare) was found to be best for imaging cells seeded on #1.5 coverslips and labelled with CMG or MTG at room temperature.
Protocol for labelling the plasma membrane:
The sample was washed once with pre warmed RPMI. The stock solution of CMG was diluted to a final concentration of 1:1000 in a pre warmed complete media and was added to the culture dish. The sample was incubated for 10 minutes. Then the was sample washed thrice with pre warmed RPMI and RPMI was replaced with imaging media before imaging.
Protocol for labelling the mitochondria:

A Stock solution was prepared by dissolving the MTG in new vial with $74.4\mu l$ of DMSO, which gave a final concentration of $1\mu M$. The sample was washed once with pre warmed RPMI. The stock solution was diluted to a final concentration of $60nM$ for staining both cell lines in A pre warmed complete media. The sample was incubated for 30 minutes with a working solution. The sample was washed with pre warmed RPMI thrice and RPMI was replaced with imaging media before imaging.

4.2.3 Fluorescence microscopy

DeltaVision OMX (GE Healthcare) is a commercial 3D-SIM set-up used in the experiments to acquire SIM images. Deconvolution microscopy can also be performed using this setup. It is equipped with 60X, 1.4NA (Olympus) oil immersion objective lens, four excitation lasers (405nm, 488nm, 561nm, 642nm) and emission filters (419-465, 500-550, 609-654, 665-705) for imaging DAPI, green, red and far red fluorophores. The images shown in this thesis are projected images of z-section stacks. Each z-section is $0.125\mu m$ and each section is illuminated 15 times (five different phases at three different angles). $15 \times 8 = 120$ images are acquired for $1\mu m$ thick sample. Image acquisition time is generally few seconds, which depends on the exposure time (typically 20-50 ms). For deconvolution microscopy, the z-section was chosen to be $0.25\mu m$ thick and $1\mu m$ thick sample is illuminated only four times. Deconvolution microscope is less phototoxic to the biological sample, but the resolution is almost half compared with SIM. Imaging was done at room temperature for maximum one hour after the cells have been taken out of the incubator. In our experiments, the thickness of samples to be imaged was kept between $1.2 - 2.5\mu m$ for SIM imaging and $4.0 - 7.0\mu m$ for deconvolution microscopy imaging. For better reconstruction of the images, oil was matched with the refractive index of coverslip before starting the experiments. This was done by checking the shape of PSF of any deconvolved image of bright point in an image. The shape should be symmetrical in all three directions. More SIM artifacts and their eradication is discussed in *Ch6*. Images were analysed using ImageJ later.

4.2.4 Quantitative phase microscopy

QPM setup is custom build by Azeem Ahmed and Vishesh Dubey, visiting PhD candidates at UiT. Discussion of this setup is beyond the scope of this thesis. I was involved in planning the experiments, sample preparation and the discussion of results. Imaging on this setup and data analysis was done by Vishesh Dubey.

4.3 Results and discussion

4.3.1 Macrophages: LPS changes sub-cellular morphology, whereas TNF-α and Con-A don't

Results for macrophages are discussed in this section will be divided into three parts. The first part will discuss the results about the morphological changes occurring in macrophages after 24 hour incubation with LPS. The second part will discuss the results about morphological changes seen at early time points of LPS-challenge. In the third part, morphological effects on macrophages challenged with TNF-α and Con-A for $24hr$ will be discussed. The experiments at early time points were not performed for TNF-α and Con-A.

24-hr incubation with LPS:

High-resolution fluorescence imaging:

Mitochondria of control and LPS-challenged macrophages were labelled with MTG and were imaged using SIM. The experiment was repeated more than three times and every time the order

of imaging the samples was different in order to eliminate the effect of time gap between imaging on the results. Each time the results were similar.

Macrophages stimulated with LPS showed different mitochondrial morphology as compared to the controls. *Fig4.1* show comparison between control and LPS-challenged macrophages. *Fig4.1)(d)* suggest that the mitochondria appear fragmented, round and shorter in LPS-challenged macrophages compared with control *Fig4.1(b)*. Distribution of mitochondria also seems different in these two cases. To rule out the phototoxicity effect due to SIM, images were also taken in DV mode and similar morphology was found in this case as well. Not all the cells seem to be affected with LPS. In order to get the statistics about the number of cells damaged, DV images of more than 150 cells were analysed. About $50 - 60\%$ cells were found to be damaged with LPS-challenge.

We discussed in *Sec3.3.1* that LPS induces large amount of NO is macrophages. The response of different cells to NO can be apoptotic or necrotic, depending on the concentration of NO they are exposed-to.[48] Apoptosis and necrosis are two different pathways of cell death. Apoptosis is natural and programmed death triggered by normal processes in our body, whereas necrosis is the premature death of cells caused by e.g., infections, toxins, etc. Recently it has been shown that the cells can die through necrosis in a programmed way. This process is known as necroptosis and is under heavy investigation.[49] Main morphological features of apoptotic cell death are: cell shrinkage, nuclear and cytoplasmic condensation. Necrosis and necroptosis share most of the morphological features, the cell and its organelles begin to swell and the membrane integrity is lost.[49] *Albina J. E. et. al.* showed that NO can induce apoptosis in case of RAW264.7 macrophages. They treated RAW264.7 macrophages with LPS ($1\mu g/ml$) in combination with INF-γ ($10U/ml$) for $48hr$ and showed using electron microscopy that nuclear and cytoplasmic condensation occurs, leading to apoptosis. They also reported that the apoptotic changes were asynchronous. Some cells were healthy and some were necrotic as well.[50, 29] *Hortelano S., et. al.* showed that NO can induce apoptosis in macrophages, also the mitochondrial membrane potential is increased.[52] *Baker B., et. al.* studied the effect of low dose ($50pg/ml$) of LPS on primary mouse macrophages and proved that low doses of LPS induces necroptosis in these cells.[28] *Kirschnek S., et. al.* co-cultured RAW264.7 macrophages with E. Coli bacteria and showed using electron microscopy that the cells die through necrosis. LPS is derived from E. Coli bacteria and they both have similar effects on macrophages.[51] Our results taken together with the results found in citations mentioned in this paragraph suggest that LPS-challenged macrophages might be headed towards necrosis. Further experiments need be done to confirm it.

Motivated by the fact that the size of macrophages seems to be increased after LPS challenge in *Fig4.1(c)*, we decided to investigate the plasma membrane of macrophages challenged with LPS. We expected some changes in the morphology of the plasma membrane. Plasma membrane of control and LPS-challenged ($1\mu g/ml$ for $24hr$) macrophages was labelled with CMG. Upon comparison of results, drastic changes were seen in the morphology. From *Fig4.2(a)* and *Fig4.2(b)* shows that the control macrophage has defined boundaries and in *Fig4.2(b)* villi-like projections can be seen on the plasma membrane. From *Fig4.2(c)* and *Fig4.2(d)* it can be seen that the cell is spreading and the membrane integrity seems to be lost. Arrows in *Fig4.2(c)* show plasma membrane rupture. Plasma membrane starts spreading out from these points, which can be seen from *Fig4.2(d)*. Thick projections can also be seen sticking out of the cell in *Fig4.2(c)*, and from *Fig4.2(d)* it can be seen that plasma membrane is spreading along these directions. Less villi-like projections from challenged cells were seen compared with the control sample. These results also indicate that the cell might be headed towards necrosis. Imaging with deconvolution microscope gave similar results thus ruling out the phototoxicity effect due to SIM on the plasma membrane.

Quantitative phase imaging:

Further studies were done using QPM. QPM is label-free imaging technique and is not

phototoxic to the cells. The results showed that the phase values and the size of LPS-challenged macrophages compared with controls. Comparing *Fig4.3* and *Fig4.4*, it can be seen that the size of cells increases more than twice. Note that *Fig4.3* and *Fig4.4* uses different pixel numbers in x and y axis. Also, the boundaries in LPS-challenged macrophage are not defined properly compared control and the cell spreads. During the experiment, the phase values of around 15 cells of (each control and LPS-challenged) macrophages were calculated and the data is plotted in *Fig4.5*. The experiment was repeated thrice and the results were similar every time. We can see from *Fig4.5* that the phase values in LPS-challenged macrophages decreased by about $2rad$. This suggests that either the thickness of the cell is decreased or the refractive index of cellular content has decreased. If we assume that the refractive index has not changed considerably, the decrease in phase value suggests that the thickness of the cell has decreased. Although another set of experiment can be performed to decouple the effect of refractive index and thickness. Thus, the surface area of a stimulated cell seems to increase and thickness seems to decrease. To the best of our knowledge, this is the first report on the quantitative phase analysis of RAW264.7 macrophages following LPS-challenge ($1\mu g/ml$ for $24hr$) using QPM. In *Fig4.4* the arrows indicate low phase regions. These can be vacuoles or membrane ruptures, and lower phase value in these regions can be due to the low refractive index as compared to rest of the cell in these areas. LPS is reported to induce vacuoles in the cytoplasm of macrophages.[53] The detailed study of these vacuole structures was done by *Yoshida K., et. al.*. [54] Using electron microscopy they showed that the vacuole structures are formed in macrophages after LPS challenge ($0.1\mu g/ml$ for 2 days). They showed that the origin of these vacuoles is not lysosomes or phagosomes, but they are related to endoplasmic reticulum or plasma membrane.

Early time-point study of macrophages challenged with LPS:

After $24hr$ stimulation studies, we were also interested in studying the effect of inflammatory agents at an early stage. NO levels reach at the lower level of detection of the Griess test later than $4hrs$. Preliminary experiments were carried out to analyse the morphological changes in macrophages at an early stage. Cells were imaged with SIM and QPM after $2hr$ and $4hr$ of LPS-stimulation. Mitochondria and plasma membrane were labelled with MTG and CMG respectively for SIM imaging. Preliminary experiments done on SIM and QPM were able to detect morphological changes as early as $2hrs$ after LPS-challenge.

High-resolution fluorescence imaging:

Comparing mitochondria in *Fig4.6* it can be seen that after $2hr$ of stimulation, mitochondrial morphology begins to change. After $2hr$ of LPS-challenge, mitochondria in 53 cells was analysed, out of which mitochondria of 14 cells changed. Mitochondria became rounded and shorter. After $4hr$, out of 58 cells, mitochondria in 18 cells seem damaged. Similarly, plasma membrane morphology also started changing just after $2hr$ of LPS-challenge. 10 out of 34 cells examined were found with damaged plasma membrane and after four hours plasma membrane structure in 7 out of 30 cells was found to be changed. We can not get general statistics because the number of cells examined in each experiment were not enough. These experiments were done twice and further experiments need to be carried out to get the statistics and to check if the experiment is reproducible. However, the initial experiments indicate that it is possible to visualise damage in mitochondria and plasma membrane at early time-points using SIM.

Quantitative phase imaging:

Fig4.8 is comparison of quantitative phase values following $0hr$, $2hr$, $4hr$ LPS-challenge. The phase values of the cells remain almost constant from $0hr$-$2hr$ and decreases by about one radian from $2hr$-$4hr$. Comparing figures *Fig4.9* and*Fig4.10* it can be seen that the size of macrophages begin to increase after two hours of LPS-challenge. Further, from *Fig4.11* we can see that the size increases further. There were also some early indications of the vacuole formation in phase images after $4hr$.

Interestingly, SIM images showed morphological changes after $2hr$, but phase values *Fig4.8*

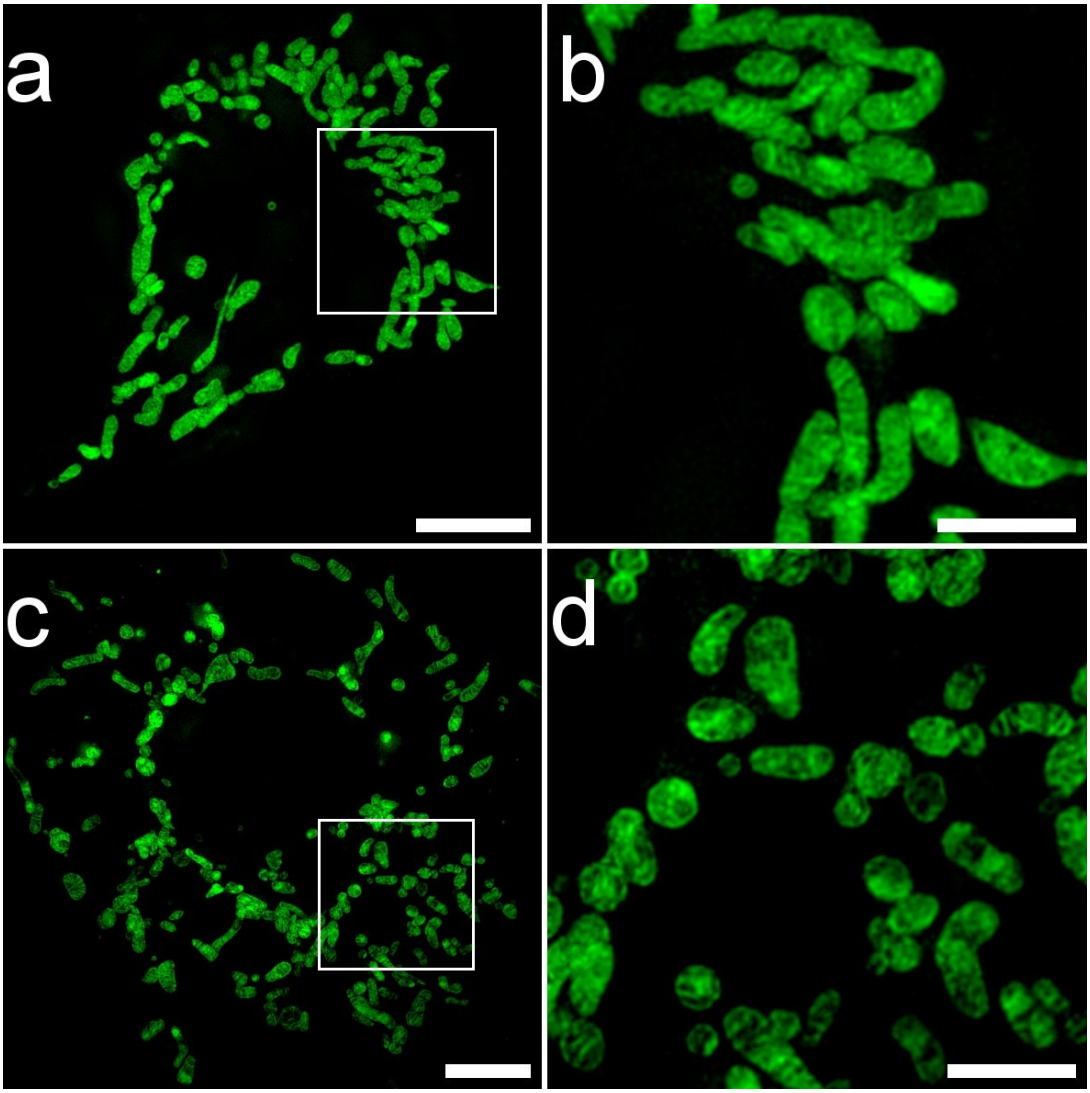

Figure 4.1: (a) and (c) 3-D projected SIM images of the mitochondria labelled with MTG ($\lambda_{ex} = 488nm$) in control and LPS-challenged macrophages, respectively. (b) and (d) are their cropped parts. Mitochondria in LPS-challenged macrophage is shorter and rounded. Scale bar: (a), (c)=$5\mu m$; (b), (d)=$2\mu m$

does not change significantly. We suspect that the phase value might be changing, but as only twenty cells were analysed, there is a probability that there was no damaged cell. Or if there are few damaged cells with lower phase value, the values must have been averaged out and thus we are not able to see in the graph. In OMX-SIM, it is easy to identify the damaged cells on mosaic, as their size is bigger than normal cell size, as the field of view due to mosaic is very large. Field of view in single mosaic is very large and typically there can be 20 macrophages in one mosaic. So the probability of getting damaged cells increase if we analyse multiple mosaics.

Effect of TNF-α and Con-A on morphology of macrophages

TNF-α-challenged and Con-A-challenged macrophages did not show any alteration in size or mitochondrial structure as compared to controls. From *Fig4.12* it can be seen that the mitochondria look similar, uniform and long. It must be noted that trophoblasts did not produce any NO following TNF-α and Con-A-challenge. Further, experiments with phase microscopy and plasma membrane using SIM were not done, as no significant changes in the mitochondrial morphology of macrophages were seen following TNF-α and Con-A-challenge in SIM images.

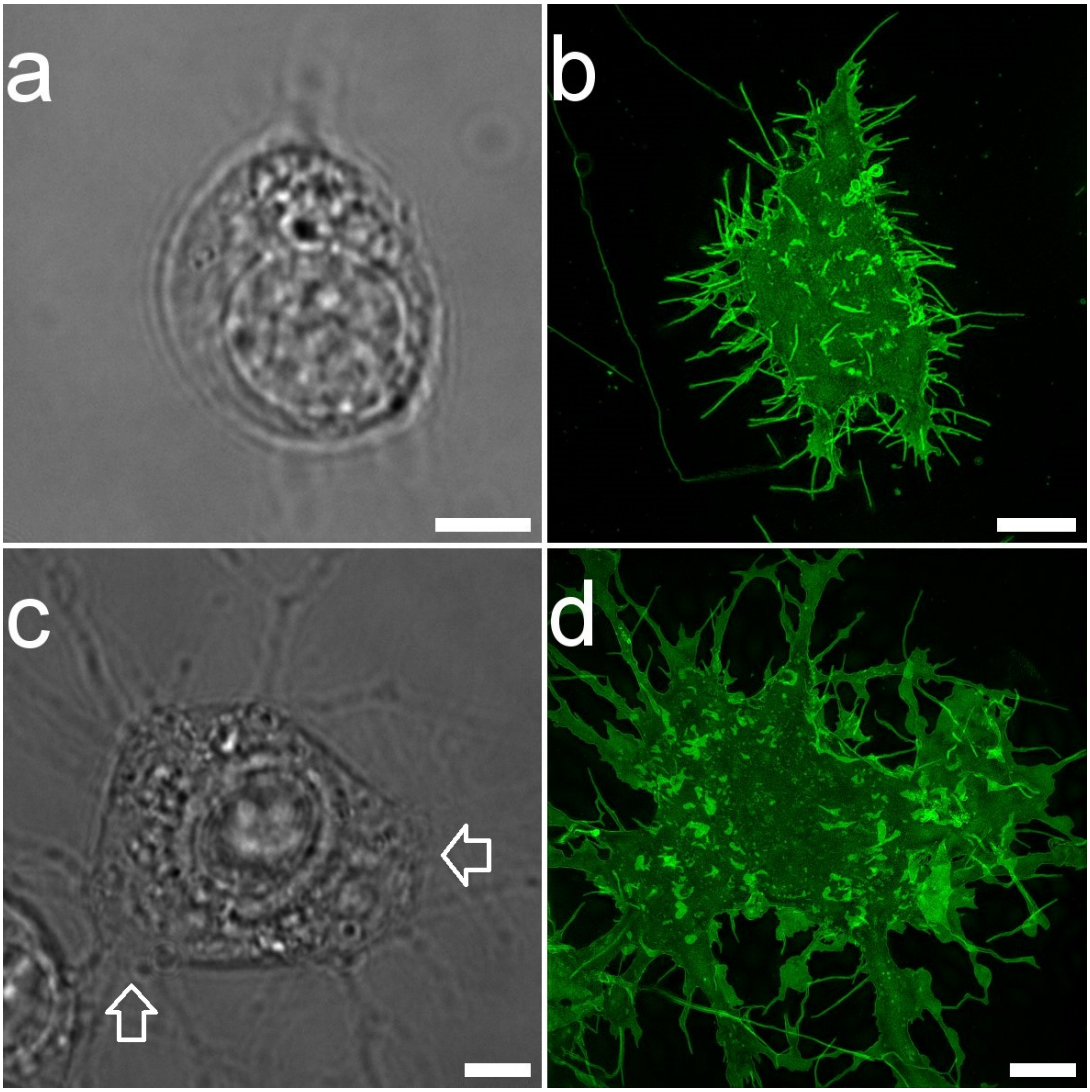

Figure 4.2: (a) and (c) bright field images of control and LPS-challenged macrophages, respectively; (b) and (d) 3-D projected images of plasma membrane labelled with CMG ($\lambda_{ex} = 488nm$) of same control and LPS-challenged macrophages. Comparing (b) and (d) one can see that the cell spreads and membrane integrity is lost in (d). Scale bar: $5\mu m$

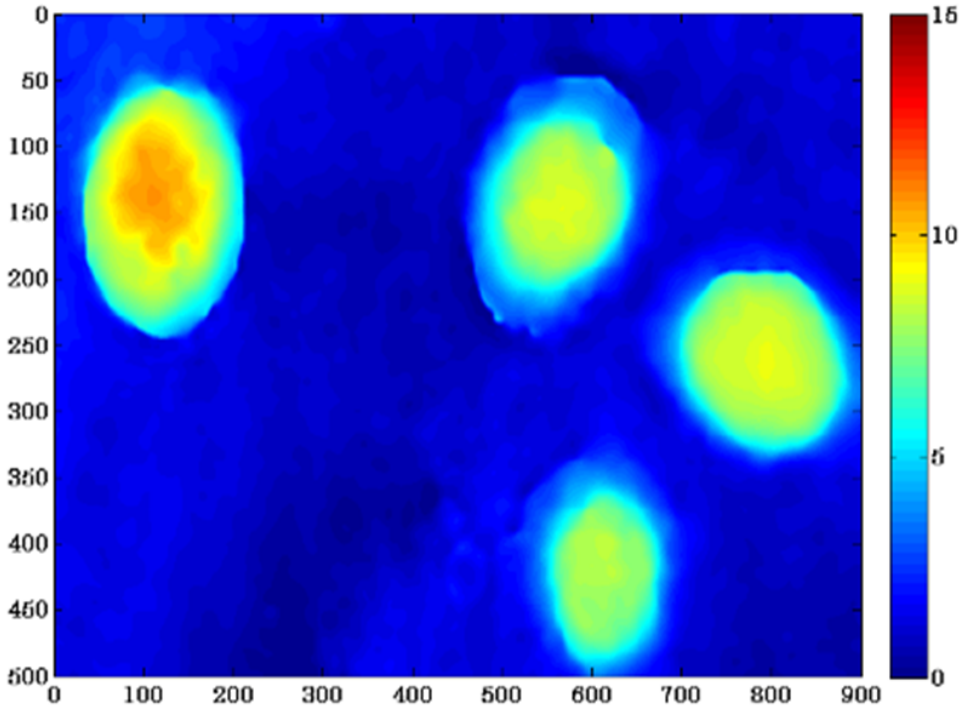

Figure 4.3: Phase image of control macrophages. x and y axes are expressed in no. of pixels and phase value is represented by the colour from 0 (blue)-15 radian (red).

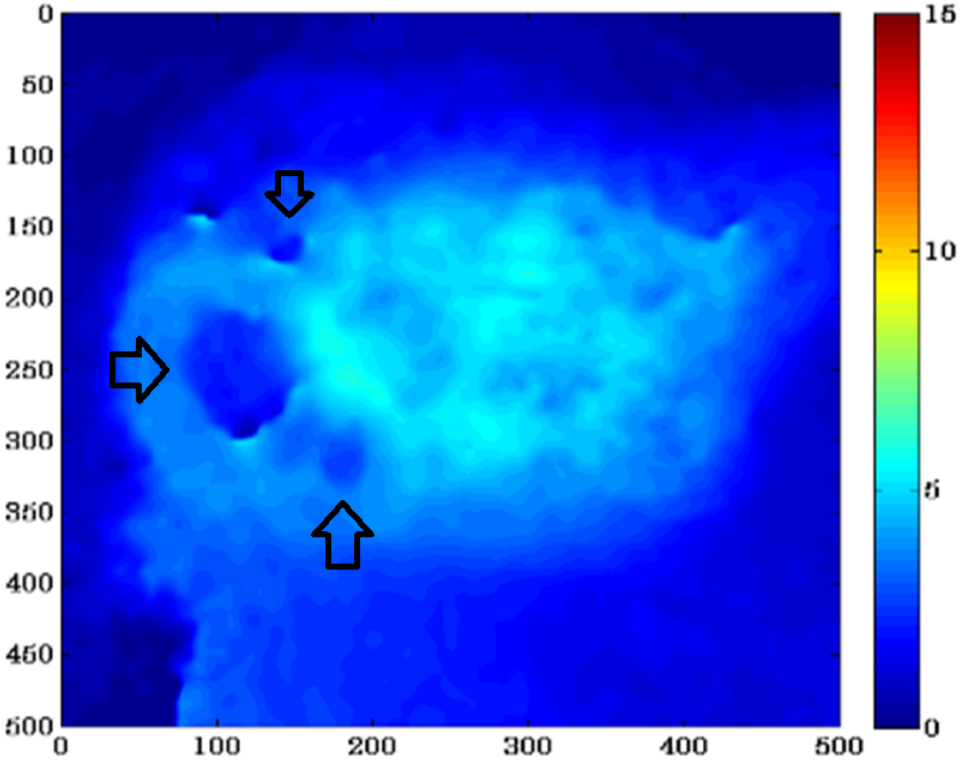

Figure 4.4: Phase image of LPS-challenged macrophage. x and y axes are expressed in no. of pixels and phase value is represented by the colour from 0 (blue)-15 radian (red). Arrows indicate the vacuole-like structures.

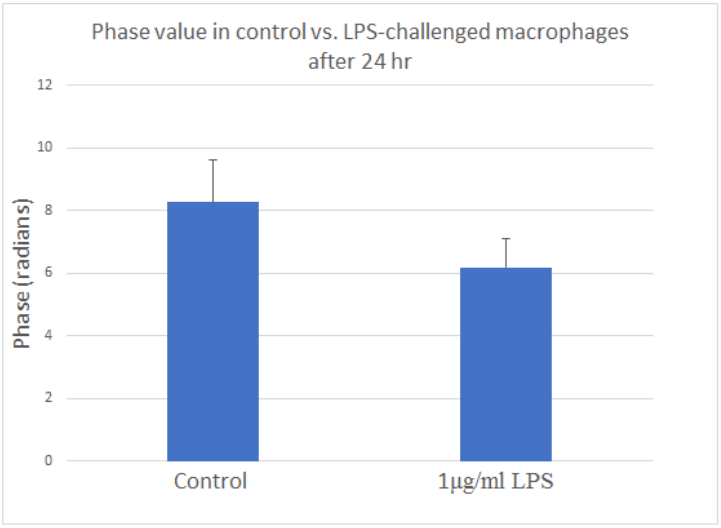

Figure 4.5: Comparison of phase values between control and LPS-challenged macrophages. Bar graph shows the mean value (+S.D.) of phase of 15-20 cells. Phase value in LPS-challenged macrophages decreased on an average 2 radians compared to control.

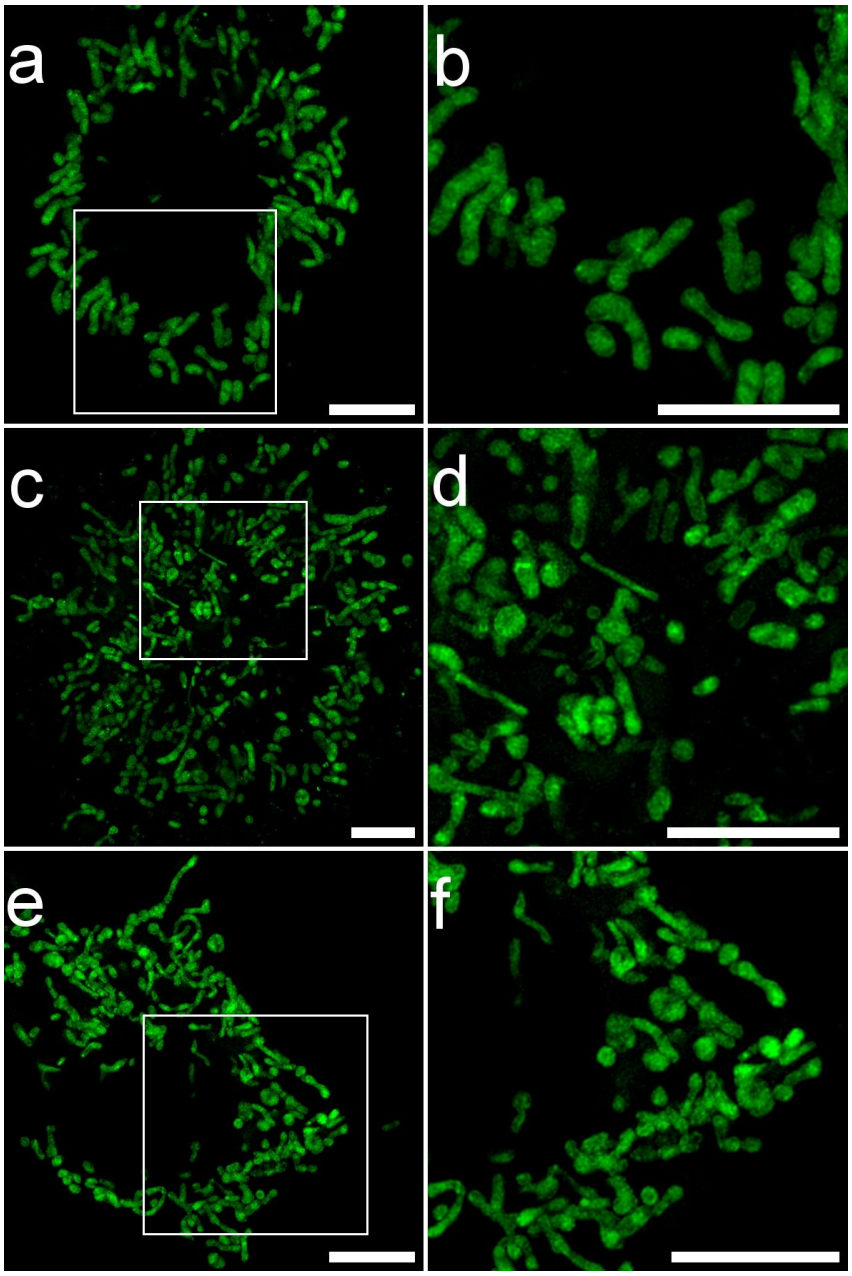

Figure 4.6: Projected 3-D images of mitochondria labelled with MTG. (a) Control, (b) $2hr$ LPS-challenged, (c) $4hr$ LPS-challenged macrophages; (b), (d) and (f) are their cropped part, respectively. Mitochondrial morphology begins to change after two hours. Scale bar: $5\mu m$

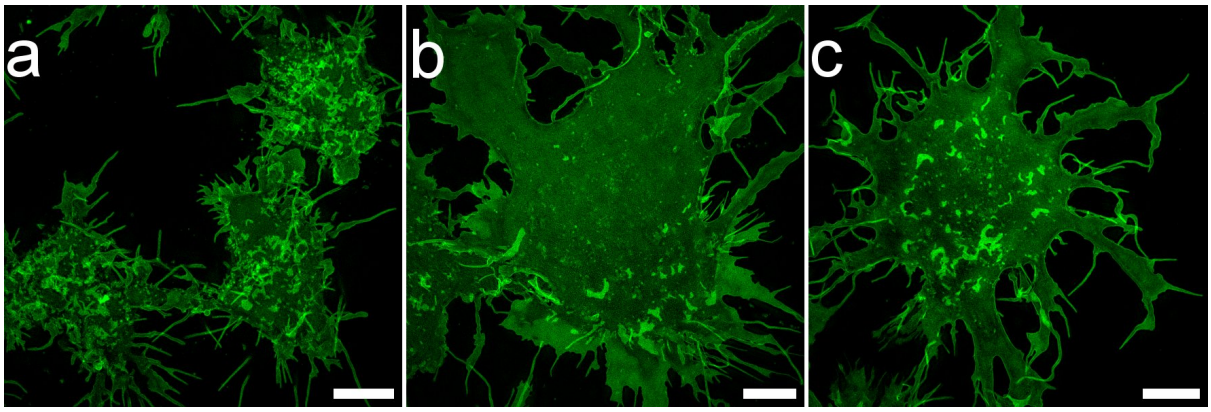

Figure 4.7: Projected 3-D images of plasma membrane labelled with CMG. (a) Control, (b) $2hr$ LPS-challenged, (c) $4hr$ LPS-challenged macrophages. Plasma membrane begins to loose its integrity after two hours. Scale bar: $5\mu m$

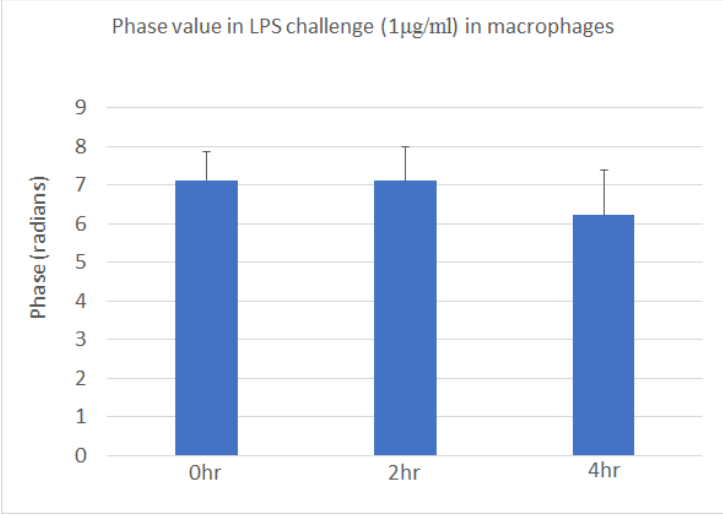

Figure 4.8: Comparison of phase values of macrophages after LPS-challenge at early time-points. Bar graph shows the mean value (+S.D.) of phase of 15-20 cells. Phase value seems constant between $0hr$-$2hr$ and starts to decrease after $2hr$.

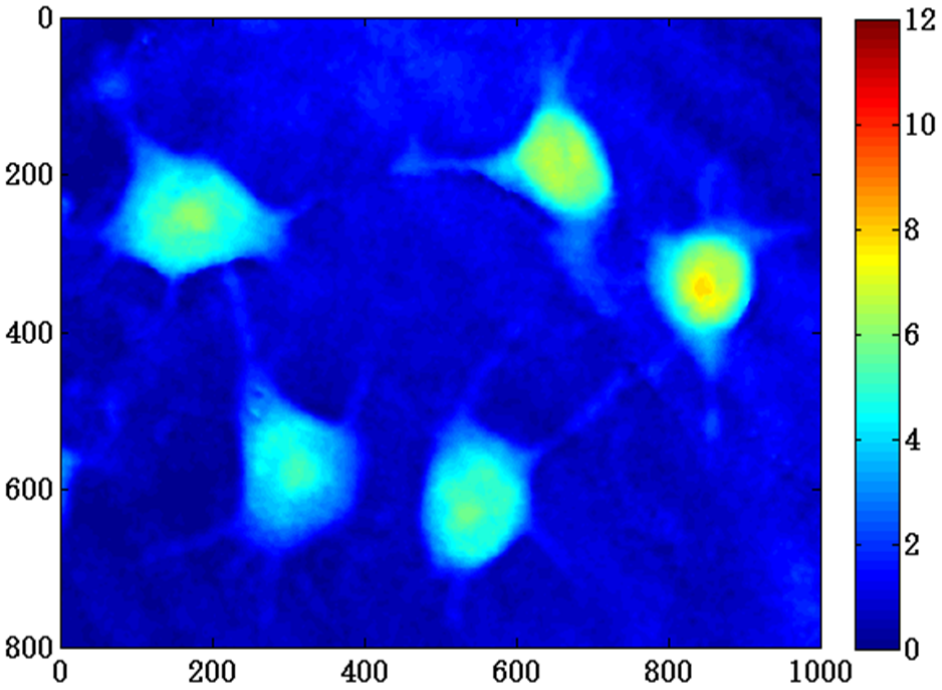

Figure 4.9: Phase image of control macrophages. x and y axes are expressed in no. of pixels and phase value is represented by the colour from 0 (blue)-15 radian (red)

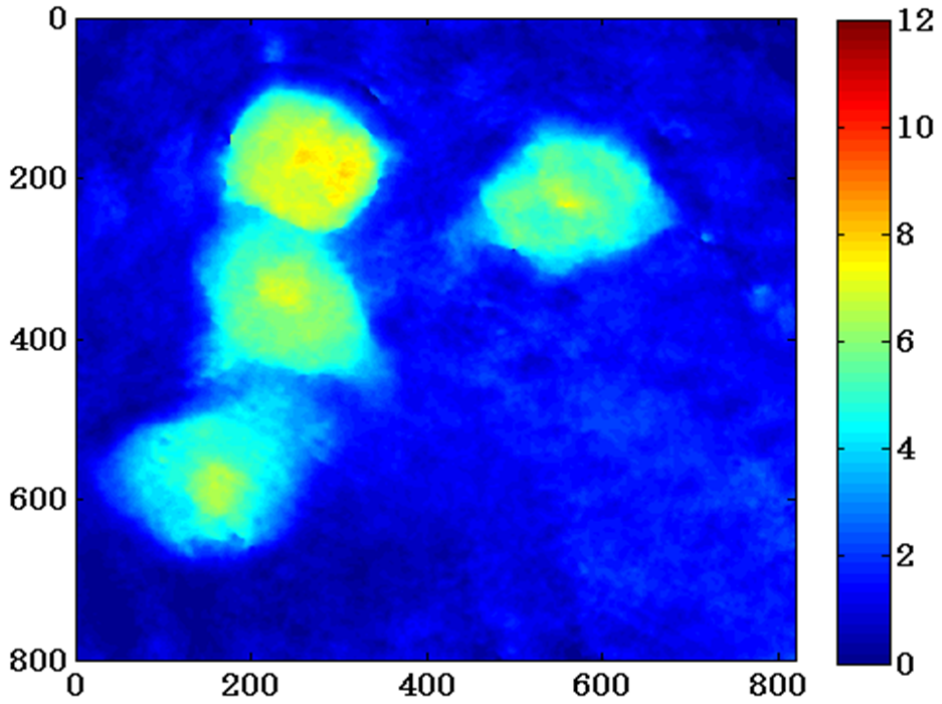

Figure 4.10: Phase image of macrophages after 2*hr* of LPS-challenge. x and y axes are expressed in no. of pixels and phase value is represented by the colour from 0 (blue)-15 radian (red). Macrophages start to spread.

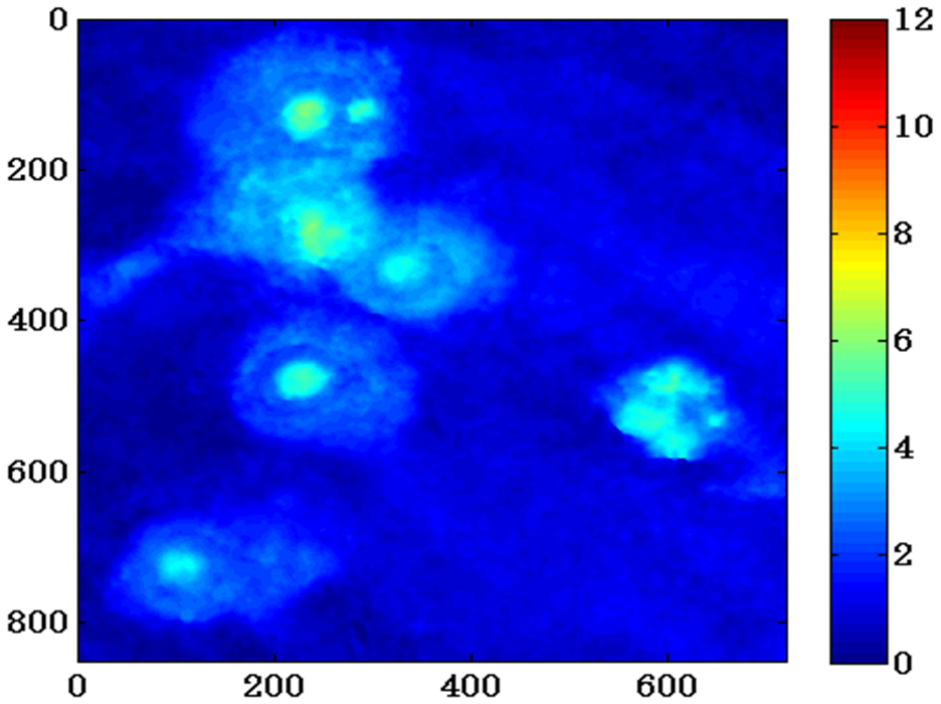

Figure 4.11: Phase image of macrophages after $4hr$ of LPS-challenge. x and y axes are expressed in no. of pixels and phase value is represented by the colour from 0 (blue)-15 radian (red). Phase values decreases as compared to control and cells are spreading.

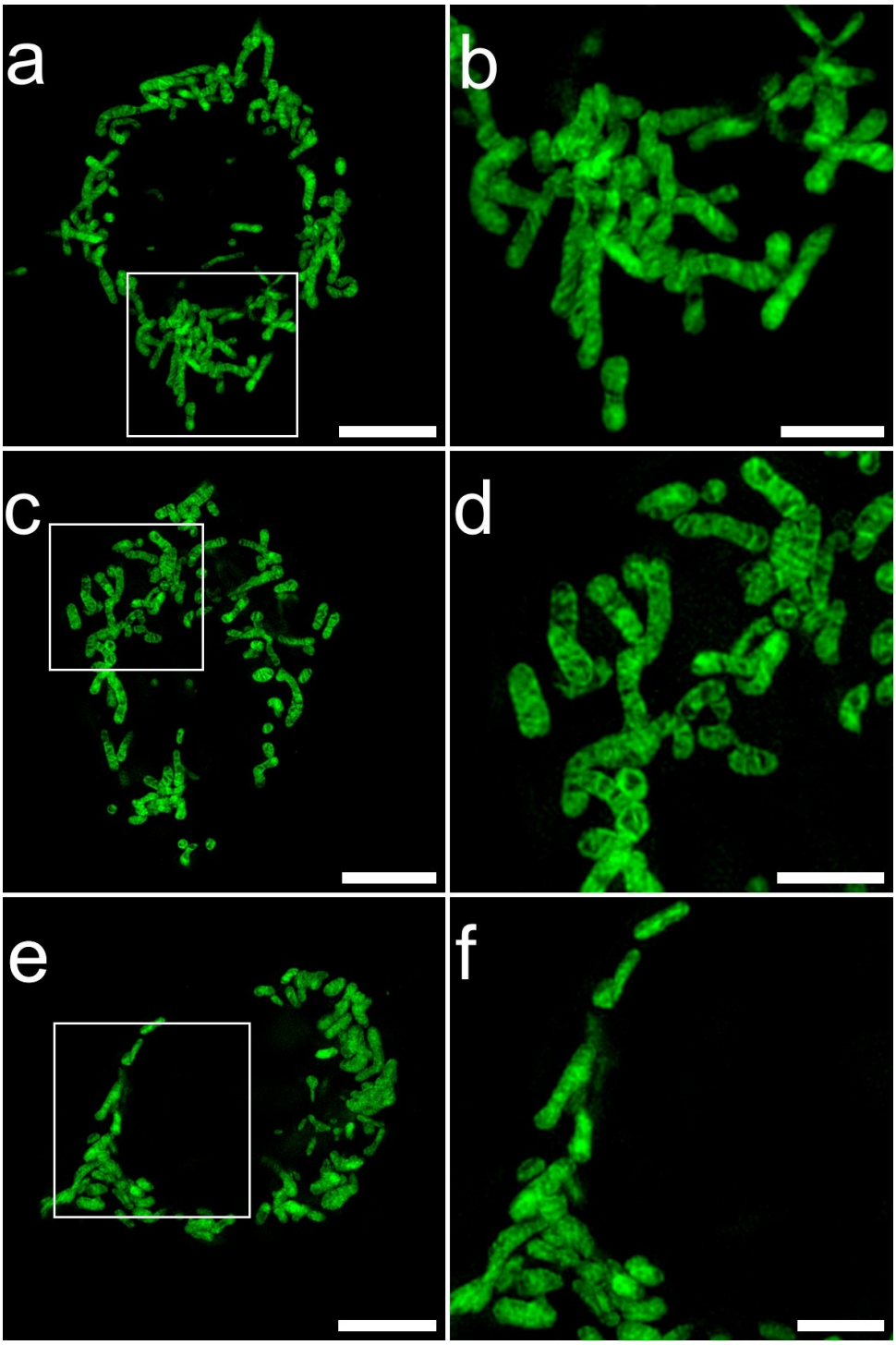

Figure 4.12: (a), (c) and (e) 3-D projected SIM images of the mitochondria labelled with MTG in control, TNF-α and Con-A-challenged macrophages, respectively. (b), (d) and (f) are their cropped parts. Mitochondria in (c) and (e) look similar to (a). Scale bar: (a), (c) and (e)=5μm; (b), (d) and (f)=2μm

4.3.2 Trophoblasts: TNF-α changes sub-cellular morphology, whereas LPS and Con-A don't

Experiments with trophoblasts were done only with $24hr$ incubation time. Due to the limited duration of master thesis, experiments with early time-point(2hr, 4hr) and QPM were not performed.

Mitochondria of control, LPS-challenged, TNF-α-challenged and Con-A-challenged trophoblasts were labelled with MTG. SIM images suggest that there are morphological differences in TNF-α-challenged trophoblasts compared with control samples. Interestingly, we could not measure increased NO production by trophoblasts after TNF-α-challenge. In *Fig4.13(d)* one can clearly see that the size of mitochondria in TNF-α-challenged trophoblasts is decreased and they appear fragmented, thicker and more in number compared with control *Fig4.13(b)*. Over 50% (36 out of 67 cells examined on SIM) showed altered mitochondrial morphology, whereas in control samples, no significant number cells were found with shorter mitochondria. This experiment was repeated three times, and morphological differences were found in TNF-α-challenged trophoblasts as compared to control samples. It would be interesting to extend the study and see what happens if we challenge the cells for a longer or shorter period.

Studies have shown that the TNF-α levels were increased in case of pregnancy complications, such as, preeclampsia.[5, 24] *Zsengellér, et. al.* reported that the mitochondria appear shorter and *Zhonghua, et. al.* showed that the mitochondria swells in preeclamptic placental tissue using electron microscopy.[55, 56] These studies taken together with our results suggest that TNF-α, which is found to be heightened in preeclamptic placenta, causes damage to mitochondria in trophoblasts.

No differences were seen in the morphology of mitochondria after challenging macrophages with LPS and Con-A compared with control. *Fig4.14(b)* and *Fig4.14(d)* suggest that the mitochondria is long and similar to mitochondria in control *Fig4.13(a)*.

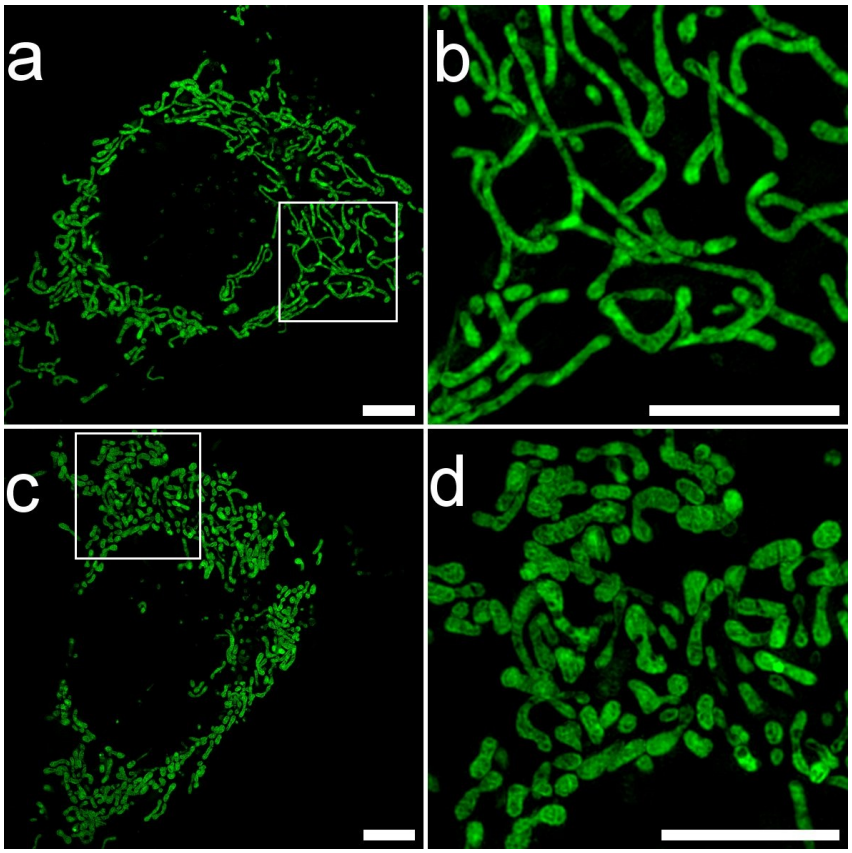

Figure 4.13: (a) and (c) 3-D projected SIM images of mitochondria labelled with MTG in control and TNF-α-challenged macrophages, respectively. (b) and (d) are their cropped parts. Mitochondria in TNF-α-challenged macrophage is shorter and thicker. Scale bar: $5\mu m$

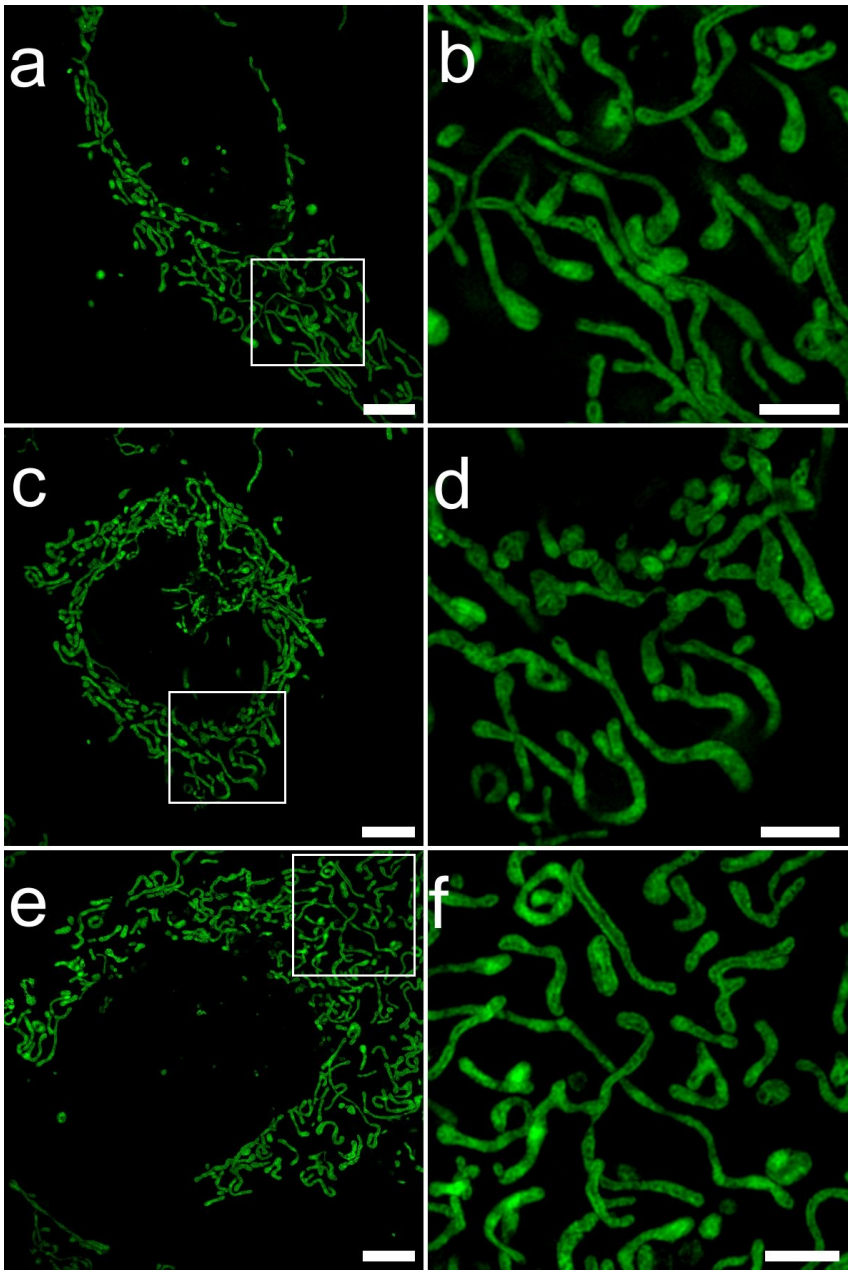

Figure 4.14: (a), (c) and (e) 3-D projected SIM images of the mitochondria labelled with MTG in control, LPS-challenged and Con-A-challenged trophoblasts, respectively. (b), (d) and (f) are their cropped parts. Mitochondrial structure in LPS-challenged and Con-A-challenged trophoblasts look similar compared to control. Scale bar: (a), (c) and (e)=5μm; (b), (d) and (f)=2μm

Chapter 5

Conclusions and perspectives

The aim of this thesis has been to study cellular and sub-cellular morphological changes in macrophages and trophoblasts in response to different inflammatory agents. From our results, we can conclude that if macrophages and trophoblasts were to be exposed to some similar inflammatory conditions, for an equal amount of time, the quantitative values of nitric oxide produced by these two are very different. Multimodal imaging results suggest that the effect of the same inflammatory agent is different, both on the cellular and sub-cellular morphology of macrophages and trophoblasts.

LPS induces significantly large amount of NO in macrophages which in turn affects the morphology of mitochondria and the plasma membrane as shown by SIM. It also affects either the thickness of the cell or the cellular content as revealed by QPM results. The Griess method does not provide cellular level information, but by using high-resolution fluorescence microscopy it was found that $50 - 60\%$ of the macrophages undergo morphological changes following $24hr$ LPS-challenge.

Through SIM and QPM it was also found that the effect on the morphology of macrophages can be observed following only $2hr$ of incubation with LPS, whereas the Griess method was unable to detect increased amount of NO before $4hr$. Damage in the plasma membrane was more prominent than in mitochondria at early time-points compared with control samples, and the size of cells started to increase following only $2hr$ of incubation with LPS.

Using The Griess method we also showed that TNF-α and Con-A were unable to induce detectable amounts of NO in macrophages. Similarly, SIM was also unable to detect any morphological changes in macrophages following TNF-α and Con-A challenge.

The Griess method showed that TNF-α was unable to induce detectable amounts of NO in trophoblasts. Interestingly, SIM showed that even though iNOS enzyme in trophoblasts is not as active compared with macrophages, TNF-α was able to alter the mitochondrial morphology in trophoblasts.

No detectable increase in NO production was reported using the Greiss method in trophoblasts following LPS and Con-A challenge. SIM also showed that there were no differences in the morphology of mitochondria after challenging macrophages with LPS and Con-A, compared with control samples.

In this thesis, we showed that SIM and QPM are live-cell friendly, useful tools to evaluate sub-cellular mechanisms associated with inflammation-mediated pregnancy complications with immense potential to explore this untouched field further for clinical applications. SIM and QPM are shown superior to the commonly used Griess reagent method in clinics to detect the inflammation at early time-points. It is important to detect inflammation as early as possible to prevent the damage caused to the body due to inflammation.

Most of the research in this field at sub-cellular level is currenlty done using electron microscopy. Electron microscopy is time consuming, highly expensive and not compatible with live-cell imaging. In contrast, SIM is faster and live-cell imaging is possible. It brings us one step closer to exploring sub-cellular mechanisms occurring in live cells. Commercially available

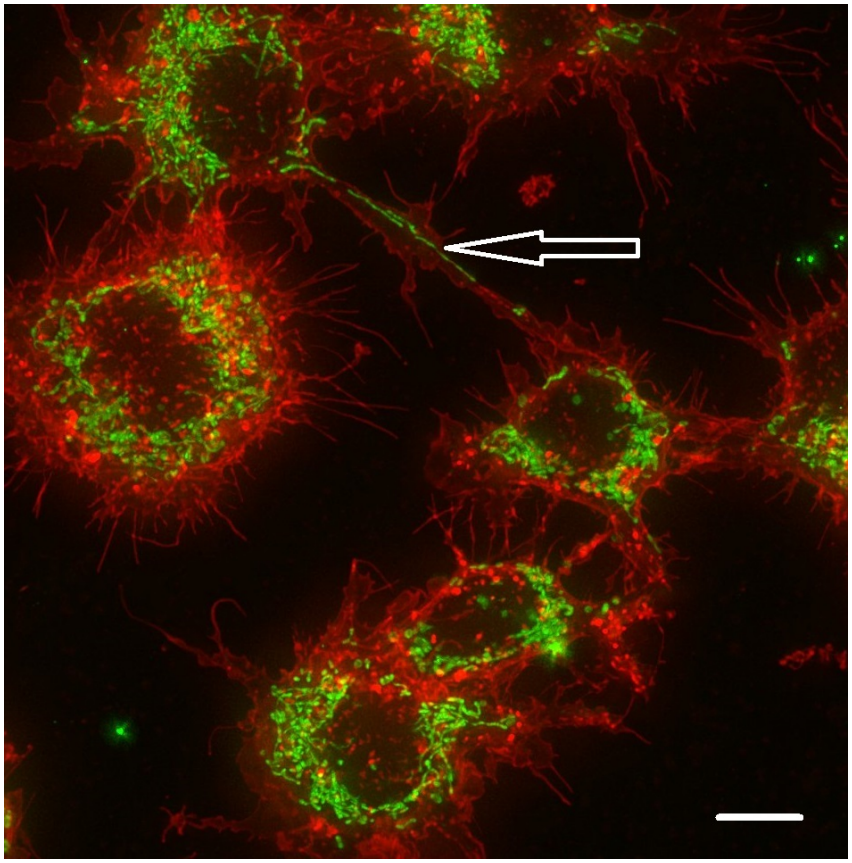

Figure 5.1: Mitochondria can be seen in the bridge (arrow) between two cells. Mitochondria might be exchanged between these cells. Scale bar: $5\mu m$

SIM setups are also highly expensive at present, which can limit the use of this technique for the possible application discussed here. The ongoing research project Chip-Based Nanoscopy at the Optical Nanoscopy research lab, UiT-The Arctic University of Norway aims at developing low cost, easy to use SIM setup with better resolution than current commercially available setups.

The present work can be extended to study primary trophoblast cells and macrophages derived from placenta. Studying them in co-culture will shed more light on their interaction with inflammatory environment. The present study of mitochondria was done using CMG, which eventually shortens the life span of cells. We can look for alternative dyes which are more photostable and non-toxic to the cells, or for label-free super-resolution techniques. It will allow us to study the mitochondrial dynamics for a longer period. This will provide a complete picture, how the dynamics change in cells exposed to inflammatory environment. In this research project, we primarily focused on detecting morphological changes in mitochondria. However, it will be interesting to study other properties of mitochondria using other dyes, e.g. JC1, which is used to study the mitochondrial transmembrane potential. LPS or TNF-α tagged with a fluorescent molecule might be used to track their path, which can increase our knowledge about the possible mechanisms by which inflammatory molecules affect the cells.

On the technique development side, it will also be interesting to combine QPM techniques with various superresolution techniques such as SIM in a single setup. This would allow us to get quantitative information about different parameters of the cell, such as its thickness . Sub-cellular morphology of the same cell can be studied using this setup.

While working with macrophages, many bridges between the cells were observed, which contained mitochondria as seem in *Fig5.1*. We hypothesize that the mitochondria is being exchanged between the cells, and this can be another important dimension of our research.

Chapter 6

Appendix

6.1 SIM artifacts

It is important to understand that SIM depends heavily upon post-image processing for the reconstruction of images. If some parameters (discussed in following sections) are not adjusted correctly, the reconstructed images can contain artifacts. These artifacts can be misleading and can be interpreted as biological features. Following section discuss about different artifacts in the SIM images, their origin and eradication.

6.1.1 Haloing

In *Fig6.1*, pseudo-pattern surrounds the real structures. This effect is called haloing effect and is caused due to refractive index mismatch between oil and the coverslip on which sample is placed.[57] Distance between an objective lens and the sample coverslip is filled with oil in order to collect more light rays. The refractive index (RI) of oil should be matched with the refractive index of coverslip to reduce losses at the interface. Haloing effects can be removed by matching the refractive index of oil and the coverslip. This is done by making the PSF symmetrical about x, y and z direction.

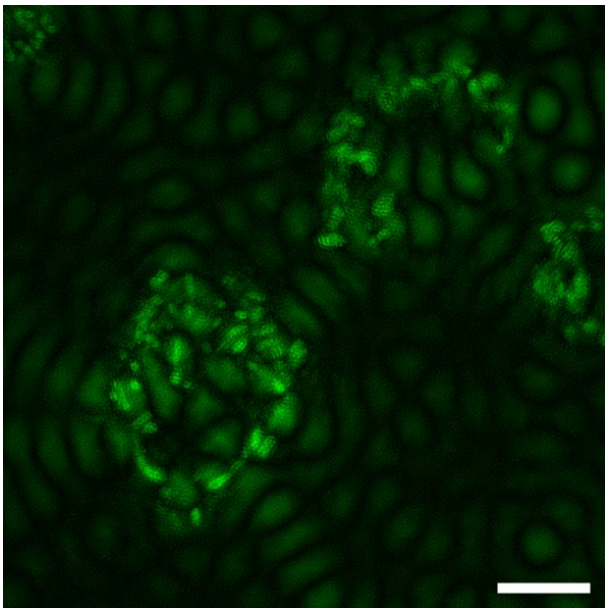

Figure 6.1: 3-D projected image of macrophages. Mitochondria was labelled with MTG. Image contain pseudo-structures surrounding the mitochondria. This was eliminated by choosing correct oil. Scale bar: Scale bar: $5\mu m$

6.1.2 Hammerstroke

Hammerstroke refers to the fine pseudo-structures (seems related to the high spacial frequencies) appearing in the reconstructed image. These are generally caused when the reconstructed noise mixes-up with poorly resolved structures. These can be misinterpreted as biological structures e.g. in image *Fig6.2b* one can think that the membrane is porous. These artifacts can be overcome by increasing signal to noise ratio.[58]

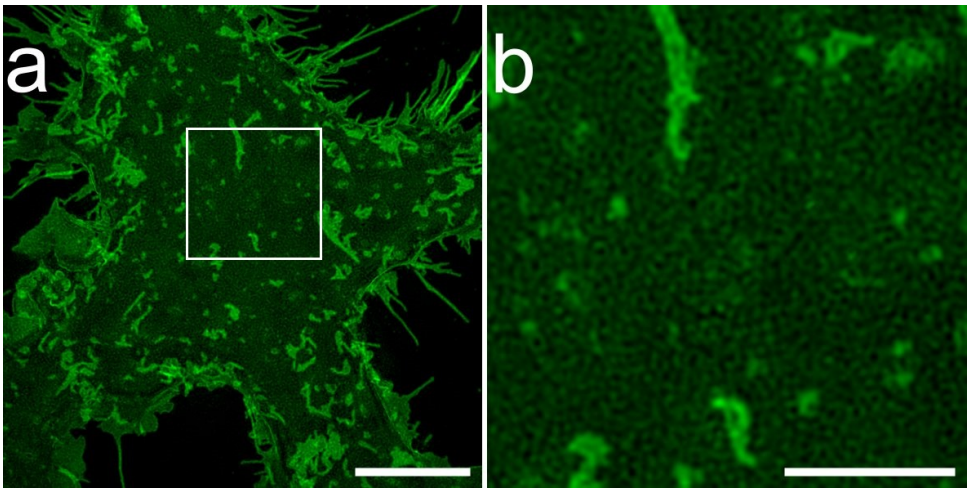

Figure 6.2: 3-D projected image of plasma membrane (labelled with CMG) of macrophage. Zooming-in reveals a fine, porous structure which is caused by the reconstructed high frequency noise. This effect is known as hammerstroke. Scale bar: (a) $5\mu m$ and (b) $2\mu m$

6.1.3 Hatching

We can see a strip pattern along one direction in the reconstructed image (*Fig6.3*). During the image acquisition in SIM, the sample is illuminated along three different angles. If settings of one or more angles is incorrect, this can lead to stripy-pattern known as hatching. This is caused by incorrect angle settings: value of one or more angles if off, leading to the formation of interference pattern above or below the focal point of objective lens; the intensity of one or more angles is low; the modulation contrast for each angle is not equally high. Correcting these angle settings can undo the hatching effect.[58]

6.1.4 Honeycomb

Fig6.4 shows the honeycomb effect which is caused by low signal to noise ratio. Low labelling density, low laser power or less exposure time can lead to these artifacts. Some dyes can loose their fluorescence properties if they were opened long before the use. Typically in our experiments if the illumination intensity 10% and the exposure time $10-40ms$ gave maximum counts around 5000, we proceeded for the experiments, otherwise the the labelling was optimised.

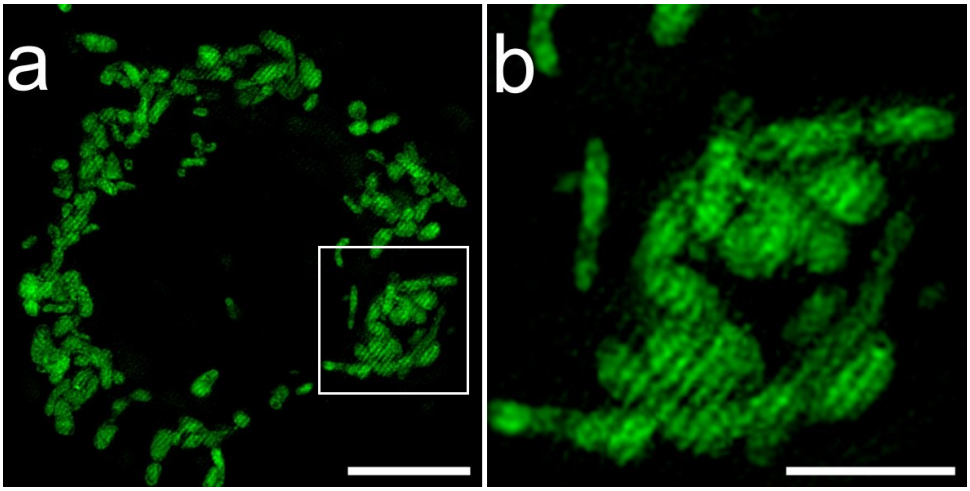

Figure 6.3: 3-D projected image of mitochondria (labelled with MTG) of macrophage. The stripy pattern is called hatching and is caused by incorect angle settings in SIM. Scale bar: (a) $5\mu m$ and (b) $2\mu m$

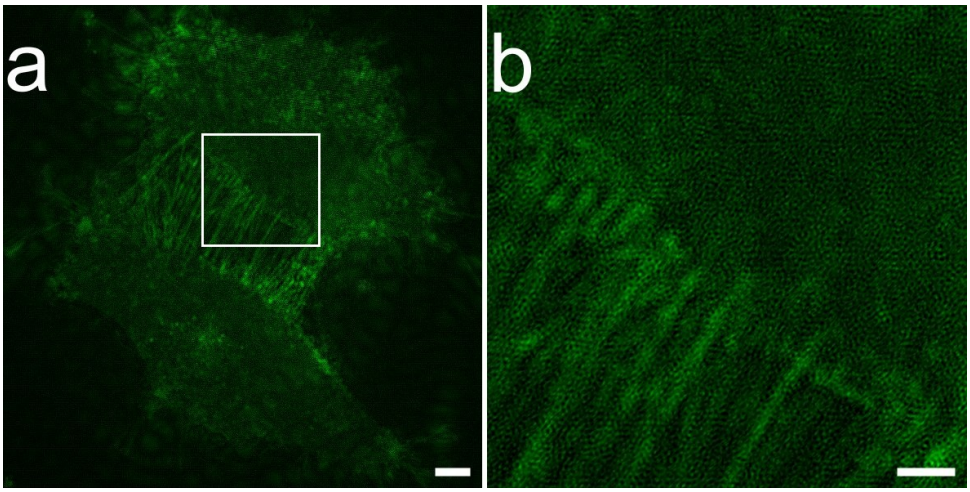

Figure 6.4: 3-D projected image of plasma membrane (labelled with CMG) of trophoblasts. The honeycomb pattern in the image caused by the low signal to noise ratio. Scale bar: (a) $5\mu m$ and (b) $2\mu m$

Chapter 7

References

[1] Robert M. S., et. al., *Lipopolysaccharide-Induced Fetal Death: The Role of Tumor-Necrosis Factor Alpha*; Biol Reprod, 50, 1108-1112, 1994. http://www.biolreprod.org/content/50/5/1108.long

[2] https://www.preeclampsia.org/health-information/149-advocacy-awareness/332-preeclampsia-and-maternal-mortality-a-global-burden

[3] Jaiswal Y.K., et. al., *Bacterial endotoxin (LPS)–induced DNA damage in preimplanting embryonic and uterine cells inhibits implantation*; Fertil. Steril., 91(5), 2095-2103, 2015. http://dx.doi.org/10.1016/j.fertnstert.2008.04.050

[4] De-Xiang X., et. al., *Effects of low-dose lipopolysaccharide (LPS) pretreatment on LPS-induced intra-uterine fetal death and preterm labor*; Toxicology, 234(3), 167-175, 2007. http://dx.doi.org/10.1016/j.tox.2007.02.010

[5] Ning F., et. al., *The Role of Decidual Macrophages During Normal and Pathological Pregnancy*; Am J Reprod Immunol, 75: 298–309, 2016.http://onlinelibrary.wiley.com/doi/10.1111/aji.12477/full

[6] Milica J. K., et. al., *MIF is among the proinflammatory cytokines increased by LPS in the human trophoblast line*; Arch Biol Sci., 68(4), 715-722, 2016. DOI:10.2298/ABS151123012J

[7] Olgun N. S., et. al., *Inhibition of Sphingosine Kinase Prevents Lipopolysaccharide-Induced Preterm Birth and Suppresses Proinflammatory Responses in a Murine Model* ; Am J of Pathology, 185(3), 862-869, 2015. http://dx.doi.org/10.1016/j.taap.2014.09.008

[8] Koga K. and Mor G., *Toll-like receptors at the maternal–fetal interface in normal pregnancy and pregnancy disorders*; Am J Reprod Immunol. 63, 587–600, 2010 http://onlinelibrary.wiley.com/doi/10.1111/aji.12258/full

[9] Cremer C., et al., *Resolution enhancement techniques in microscopy*; EPJ H 38, 281, 2013. http://link.springer.com/article/10.1140/epjh/e2012-20060-1

[10] http://news.mit.edu/2012/discovering-when-cells-divide-0806

[11] Jost A. and Heintzmann R., *Superresolution Multidimensional Imaging with Structured Illumination Microscopy*; Annu. Rev. Mater. Res. 43, 261–82, 2013. http://www.annualreviews.org/doi/abs/10.1146/annurev-matsci-071312-121648

[12] Hell S. W. and Wichmann J., *Breaking the diffraction resolution limit by stimulated emission: stimulated-emission-depletion fluorescence microscopy*; Opt. Lett. 19, 780-782, 1994. https://www.osapublishing.org/ol/abstract.cfm?uri=ol-19-11-780

[13] http://www.spielberg-ocr.com/printing.html

[14] Ulrich Kubitscheck, *Fluorescence Microscopy: From Principles to Biological Applications*; Wiley-Blackwell, Germany, 2013. http://eu.wiley.com/WileyCDA/WileyTitle/productCd-3527329226.html

[15] Best G., et. al., *Structured illumination microscopy of autofluorescent aggregations in human tissue*; Micron, 42, 330–335, 2011. http://www.sciencedirect.com/science/article/pii/S096843281000212X

[16] Peng X., *Optical Nanoscopy and Novel Microscopy Techniques*; CRC Press, 2015 https://www.crcpress.com/Optical-Nanoscopy-and-Novel-Microscopy-Techniques/Xi/p/book/9781466586291

[17] Oddone,A et. al., *Super-Resolution Imaging With Stochastic Single-Molecule Localization: Concepts, Technical Developments, and Biological Applications*; Microsc Res Tech, 77, 502-509, 2014. http://onlinelibrary.wiley.com/doi/10.1002/jemt.22346/full

[18] Oddone A., et. al. *Super-Resolution Imaging With Stochastic Single-Molecule Localization: Concepts, Technical Developments, and Biological Applications*; Microsc Res Tech, 77, 502–509, 2014. http://onlinelibrary.wiley.com/doi/10.1002/jemt.22346/full

[19] Weisenburger S. and Sandoghdar V., *Light microscopy: an ongoing contemporary revolution*; Contemp Phys, 56, 123-143, 2015. https://arxiv.org/abs/1412.3255

[20] Blom H. and Brismar H., *STED microscopy: increased resolution for medical research?*. J of Int Med, 276, 560–578, 2014. http://onlinelibrary.wiley.com/doi/10.1111/joim.12278/full

[21] Hell, S.W., *Microscopy and its focal switch;* Nat. Methods, 6, 24-32, 2009. http://www.nature.com/nmeth/journal/v6/n1/full/nmeth.1291.html

[22] https://en.wikipedia.org/wiki/Phase-contrast_microscopy#/media/File:Phase_shift_image_of_cells_in_3D.jpg

[23] Moore K. L., et. al., *The developing human : clinically oriented embryology*; Elsevier, 10th ed., USA, 2015. https://www.amazon.com/Developing-Human-Clinically-Oriented-Embryology/dp/1437720021

[24] Renaud S. J. and Graham C. H., *The Role of Macrophages in Utero-placental Interactions During Normal and Pathological Pregnancy*; Cell Mol Immunol; 37, 535-564, 2008. http://dx.doi.org/10.1080/08820130802191375

[25] James J. L., et. al., *The regulation of trophoblast migration across endothelial cells by low shear stress: consequences for vascular remodelling in pregnancy*; Cardiovasc Res 93 (1), 152-161, 2012. doi: 10.1093/cvr/cvr276

[26] Kaufmann P., et. al., *Endovascular Trophoblast Invasion: Implications for the Pathogenesis of Intrauterine Growth Retardation and Preeclampsia*; Biol Reprod, 69 (1), 1-7, 2003. https://academic.oup.com/biolreprod/article-lookup/doi/10.1095/biolreprod.102.014977

[27] Seminara A. R., et. al., *LPS/IFN-γ-Induced RAW 264.7 Apoptosis is Regulated by Both Nitric Oxide–Dependent and –Independent Pathways Involving JNK and the Bcl-2 Family*;Cell Cycle, 6(14), 1772-1778, 2007. http://www.tandfonline.com/doi/abs/10.4161/cc.6.14.4438

[28] Baker B., et. al. *Molecular and Cellular Mechanisms Responsible for Cellular Stress and Low-grade Inflammation Induced by a Super-low Dose of Endotoxin*; JBC, 289, 16262-16269, 2014. http://www.jbc.org/content/289/23/16262.full

[29] Albina J. E., et. al., *Nitric Oxide-Mediated Apoptosis in Murine Peritoneal Macrophages*; J immnol 150(11), 5080-5085, 1993 http://www.jimmunol.org/content/jimmunol/150/11/5080.full.pdf

[30] Haider S. and Knofler M., *Human Tumour Necrosis Factor: Physiological and Pathological Roles in Placenta and Endometrium*; Placenta 30, 111–123, 2009. http://www.sciencedirect.com/science/article/pii/S0143400408003524

[31] http://www.jamequist.umn.edu/Protocols/Con%20A%20stimulation.htm

[32] Hirvonen M. R., et. al., *Heat shock proteins and macrophage resistance to the toxic effects of nitric oxide*; Biochem J, 315(3); 845-849, 1996. http://www.biochemj.org/content/315/3/845

[33] Ohki K., et. al., *Suppressive effects of serum on the LPS-induced production of nitric oxide and TNF-alpha by a macrophage-like cell line, WEHI-3, are dependent on the structure of polysaccharide chains in LPS*, Immunol Cell Biol, 77, 143–152, 1999. https://www.nature.com/icb/journal/v77/n2/full/icb199918a.html#bib19

[34] Asagiri K., et. al., *Involvement of peroxynitrite in LPS-induced apoptosis of trophoblasts*; J. Obstet. Gynaecol. Res., 29(1), 49–55, 2003. http://onlinelibrary.wiley.com/doi/10.1046/j.1341-8076.2003.00066.x/full

[35] Parameswaran N. and Patial S., *Tumor Necrosis Factor-alpha Signaling in Macrophages*; Crit Rev Eukaryot Gene Expr, 20(2), 87-103, 2010. https://www.ncbi.nlm.nih.gov/pmc/articles/PMC3066460/

[36] Lin J. Y., et. al., *Tumor necrosis factor alpha augments nitric oxide-dependent macrophage cytotoxicity against Entamoeba histolytica by enhanced expression of the nitric oxide synthase gene*; Infect and Immun, 62(5), 1534-1541, 1994. https://www.ncbi.nlm.nih.gov/pmc/articles/PMC186349/

[37] Dwyer J. M. and Johnson C., *The use of concanavalin A to study the immunoregulation of human T cells*; Clin Exp Immunol. 46(2), 237-249, 1981. https://www.ncbi.nlm.nih.gov/pmc/articles/PMC1536405/?page=1

[38] Tian L., et. al., *Activated T cells enhance nitric oxide production by murine splenic macrophages through gp39 and LFA-l*; Eur. J. Immunol, 25, 306-309, 1995. http://onlinelibrary.wiley.com/doi/10.1002/eji.1830250152/epdf

[39] Faas M. M., et. al., *Monocytes and macrophages in pregnancy and pre-eclampsia*; Front. Immunol., 298 (5), 2014 https://doi.org/10.3389/fimmu.2014.00298

[40] Holland O., et. al., *Review: Placental mitochondrial function and structure in gestational disorders*; Placenta, in press, 2016 http://doi.org/10.1016/j.placenta.2016.12.012

[41] Wu F., et. al., *Oxidative stress: placenta function and dysfunction*; Am J Reprod Immunol. 76, 258–271, 2016. http://onlinelibrary.wiley.com/doi/10.1111/aji.12454/full

[42] Detmer S. A. and Chan D. C., *Functions and dysfunctions of mitochondrial dynamics*;Nature Reviews Molecular Cell Biology 8, 870-879 (2007). http://www.nature.com/nrm/journal/v8/n11/full/nrm2275.html

[43] James, A. M. and Murphy M. P., *How mitochondrial damage affects cell function*; J Biomed Sci, 9, 475-487, 2002. https://link.springer.com/article/10.1007/BF02254975

[44] Cuschieri J. and Maier R.V., *Oxidative Stress, Lipid Rafts, and Macrophage Reprogramming*; 9(9), 1485-1498, 2007. http://online.liebertpub.com/doi/abs/10.1089/ars.2007.1670

[45] Danielsen, E.M., *Probing endocytosis from the enterocyte brush border using fluorescent lipophilic dyes: lipid sorting at the apical cell surface*; Histochem Cell Biol 143, 545, 2015. https://link.springer.com/article/10.1007%2Fs00418-014-1302-2

[46] Jacobs S., *High resolution imaging of live mitochondria*; Biochimica et Biophysica Acta 1763, 561–575, 2006. http://www.sciencedirect.com/science/article/pii/S0167488906000838

[47] Chazotte B., *Labeling Mitochondria with MitoTracker Dyes*; Cold Spring Harb Protoc 2011; http://cshprotocols.cshlp.org/content/2011/8/pdb.prot5648.long

[48] Peter K. M., et. al., *The regulatory role of nitric oxide in apoptosis*; Int Immunopharmacol, 1, 1421-1441, 2001. http://www.sciencedirect.com/science/article/pii/S1567576901000881

[49] Martin S. J. and Henry C. M., *Distinguishing between apoptosis, necrosis, necroptosis and other cell death modalities*; 61(2), 87-89, 2013. http://www.sciencedirect.com/science/article/pii/S104620231300193X

[50] Albina J.E., and Reichner J.S., *Role of nitric oxide in mediation of macrophage cytotoxicity and apoptosis*; Cancer Metastasis Rev, 17, 39, 1998. https://link.springer.com/article/10.1023%2FA%3A1005904704618?LI=true

[51] Kirschnek S., et. al., *Necrosis-like cell death induced by bacteria in mouse macrophages*; Eur. J. Immunol. 2004. 34: 1461–1471. http://onlinelibrary.wiley.com/doi/10.1002/eji.200324582/pdf

[52] Hortelano S., et. al. *Induction of apoptosis by nitric oxide in macrophages is independent of apoptotic volume decrease*; Cell Death and Differentiation, 9, 643 - 650, 2002. https://www.nature.com/cdd/journal/v9/n6/pdf/4401017a.pdf

[53] Amano F. and Akamatsu, Y., *A Lipopolysaccharide (LPS)-Resistant Mutant Isolated from a Macrophagelike Cell Line, J774.1, Exhibits an Altered ActivatedMacrophage Phenotype in Response to LPS* ; Infect Immun, 2166-2174, 1991. http://iai.asm.org/content/59/6/2166.full.pdf

[54] Yoshida K., et. al., *Lipopolysaccharide-induced vacuoles in macrophages: Their origin is plasma membrane-derived organelles and endoplasmic reticulum, but not lysosomes*; J Endotoxin Res, 5(3), 1999. http://journals.sagepub.com/doi/abs/10.1177/09680519990050030601

[55] Zsengellér Z. K., et. al. *Trophoblast mitochondrial function is impaired in preeclampsia and correlates negatively with the expression of soluble fms-like tyrosine kinase 1*; An Int J Women's Cardiovascular Health 6, 313–319, 2016. http://www.sciencedirect.com/science/article/pii/S2210778915300325

[56] Sji, Z., et. al., *Comparative proteomics analysis suggests that placental mitochondria are involved in the development of pre-eclampsia.*; PLoS One 8(5), e64351, 2013. https://doi.org/10.1371/journal.pone.0064351

[57] http://www.indiana.edu/~lmic/Workshops/LocalizationMicroscopy/Web/2015_05_26%20Indiana%20SIM%20copy.pdf

[58] Demmerle J., et. al., *Strategic and practical guidelines for successful structured illumination microscopy*; Nature Protocols 12, 988–1010, 2017. https://www.nature.com/nprot/journal/v12/n5/full/nprot.2017.019.html